Investigating the Diurnal Cycle in 9 km ECMWF Potential Vorticity Variability in the Upper Troposphere and Lower Stratosphere over Gulf Coast Tropical Cyclones

Daniel J. Fortier Jr.

A Thesis submitted in partial fulfillment of the requirements for the degree of

Master of Science

(Atmospheric and Oceanic Sciences)

at the University of Wisconsin Madison

Abstract

ECMWF high resolution (~ 9 km) operational forecast analyses of potential vorticity (PV) are used to explore the diurnal cycle of Gulf Coast tropical cyclones (TCs) during 2020 – 2022. The standard deviation of PV, σ_{PV}, within horizontal domains centered on each TC is calculated at the 100 hPa pressure level. A case study of TC Marco, plus two composites (all 2020 Gulf of Mexico TCs and all 2020 – 2022 Gulf of Mexico TCs) are described in this thesis.

The upper troposphere/lower stratosphere (UTLS) is a focal region of interest since σ_{PV} exhibits a maximum at the base of the stratosphere above TCs. Variability of PV in the UTLS is related to updrafts in the TC. A noticeable diurnal cycle in σ_{PV} was seen in the case study of TC Marco. Marco having never reached an intensity of category 2 (C2) over its lifespan, while also never making full landfall, was expected to have maximum values of σ_{PV} around sunrise, which proved to be true for most of the days studied. An annulus method described showed that maxima in σ_{PV} at 100 hPa also did not propagate outward from the center of the storm over the course of the day.

The composite studies of Gulf Coast TCs showed a noticeable, yet not statistically significant, diurnal cycle in σ_{PV} at 100 hPa for C2 or stronger TCs, with maxima around midnight. A weaker diurnal cycle was observed when looking at C1 or weaker TCs, with maxima closer to sunrise. The inner ring of mature hurricanes showed a statistically significant diurnal cycle in σ_{PV} at 100 hPa, with peaks aligning with the hypothesized maxima near midnight. This was expected, as σ_{PV} is tied to the location of the updrafts in convection. Convection near the center

of TCs exhibited a stronger diurnal cycle. This midnight maximum is consistent with radiative theories of the cloud greenhouse effect.

Acknowledgements

I would like to thank Dr. Matthew Hitchman for taking a statistics nerd under his wing and showing him just how interesting our atmosphere is. I am thankful for all our discussions, whether they were research related or not, as each one made me critically think and gave me the passion to learn more about this subject. Thank you to Shellie Rowe for creating this project, and for helping me in many various ways throughout the process of this research. Thank you to Sadie and Xander. Two of the best friends a boy could have. I miss you both, but I know you are in a better place. Love you two. Thank you to Pete for always being there to help with IT aspects of this project and thank you to Dr. Maroon and Rudra for coding help. Also thank you to my parents, who have helped me through some rough times and have always been by my side. Thank you to Coach Hall, and everyone in the Saint Michael's Athletics Department. You all helped me learn how to lead, and instilled a confidence in me which has helped me throughout all aspects of my life. Thank you to all my friends within the AOS department, especially my lab mate Yingshun for all the discussions, whether they be science related or not. Lastly thank you to my readers, Dr. Maroon and Dr. Martin. This work was supported by NSF grant AGS-1947658.

The greatest pleasure in life

is doing what people say you cannot do.

WALTER BAGEHOT

Table of Contents

List of Figures

List of Tables

Chapter 1. Introduction

Tropical cyclones are strong, tropical, low-pressure systems that harm many communities worldwide. Due to their strength and consequences, these storms have long been researched. Recently, research has begun to highlight the diurnal cycle of hurricanes. The diurnal cycle of a hurricane is the variation in storm strength and structure throughout a day. Even with the increased scrutiny of the diurnal cycle, many questions remain unanswered, such as how well high-resolution models are predicting this cyclic nature.

This study sets out to examine the diurnal cycle of potential vorticity (PV) variability in the upper troposphere/lower stratosphere (UTLS) found in the European Centre Medium Range Weather Forecasts IFS High-Resolution Operational Forecasts for tropical cyclones in the Gulf of Mexico. The original focus of this study was the record-breaking 2020 Atlantic Hurricane season. However, the focus then expanded to include both 2021 and 2022 Gulf of Mexico tropical cyclones to allow for stronger statistical statements.

In this thesis, storms will be classified using the National Hurricane Center (NHC) and the Saffir Simpson Scale. Table 1.1 presents the classifications and the wind speed range of each category. A tropical depression is an organized tropical cyclone with winds up to 38 mph. A tropical storm has winds between 39 and 73 mph, and a hurricane is classified as any tropical cyclone with winds exceeding 74 mph.

Classification	Wind Speed (MPH)	Abbreviation used in this thesis
Tropical Depression	≤ 38 mph	TD
Tropical Storm	≥ 39 mph ≤ 73 mph	TS
Category 1 Hurricane	≥ 74 mph ≤ 95 mph	C1
Category 2 Hurricane	≥ 96 mph ≤ 110 mph	C2
Category 3 Hurricane	≥ 111 mph ≤ 129 mph	C3
Category 4 Hurricane	≥ 130 mph ≤ 156 mph	C4
Category 5 Hurricane	≥ 157 mph	C5

Table 1.1. Naming conventions for classifying tropical cyclone strength in the Atlantic basin.

1.1. The Historic 2020 Atlantic Hurricane Season

The 2020 Atlantic hurricane season is chosen for study because it was an overly active storm season, especially in the Gulf of Mexico. In total, a record-breaking 30 named storm systems occurred during the 2020 Atlantic hurricane season (Reed et al., 2022), along with 14 such storms reaching the criteria for a Category 1 or stronger hurricane. The first major hurricane of the season, Hurricane Laura, occurred in late August. Laura was the most damaging of the 2020 landfalling storms (Probst et al., 2021), accounting for over $18 billion according to AON's 2020 Annual Report (2021). Four of the top ten global economic loss events in 2020 are tied to the Atlantic Hurricane Season (2020 Annual Report), with Laura being the second most costly event overall.

1.1.1 2020 Gulf of Mexico

Many (nine) of the storms during the 2020 Atlantic hurricane season crossed through the Gulf of Mexico and made landfall along the Gulf Coast, making the basin intriguing to study. Not only were there many storms that went through the Gulf, but many had very similar tracks and made landfall (or neared land) very close to each other. Out of the nine storms in the Gulf, four (Cristobal, Laura, Delta, and Zeta) made landfall along the coast of Louisiana, with a fifth (Marco) dissipating right off the coast (Blackwell 2020).

Hurricane Name	Date of Storm
Hanna	July 23 – 26
Laura	August 20 – 29
Marco	August 21 – 25
Sally	September 11 – 17
Gamma	October 2 – 6
Delta	October 4 – 10
Zeta	October 24 – 29
Eta	October 31 – November 13
Iota	November 13 – 18

Table 1.2. Hurricanes used in creating a composite of 2020 Gulf of Mexico storms.

In this study, composites were created for analysis, including tropical cyclones in the Gulf of Mexico that intensified to a Category 1 or stronger hurricane. Table 1.2 shows each storm in 2020 that met this criterion and was thus used in the results found in this thesis.

1.1.2. Further Storms Included

To further our analysis, additional storms were added to the composite (Table 1.3). Each of these storms passed through the Gulf of Mexico in either 2021 or 2022 and reached an intensity of Category 1 or stronger. These two hurricane seasons were not as active as the 2020 hurricane season, but added six additional storms, bringing the total storms included in this research to 15.

Hurricane Name	Date of Storm
Elsa	June 30 – July 9, 2021
Grace	August 13 – 21, 2021
Ida	August 26 – September 1, 2021
Nicholas	September 12 – 15 , 2021
Ian	September 23 – 30, 2022
Lisa	October 31 – November 5, 2022

Table 1.3. Additional hurricanes included in a composite from 2021 and 2022.

1.2. Motivation: The Diurnal Cycle in Past Research

Prior to research looking at the diurnal cycle of tropical cyclones, the diurnal cycle of other forms of tropical rainfall and convection was found to peak in the early morning around 6 AM local time, with a minimum after sunset (Gray and Jacobson, 1977). Jiang et al. (2011) binned data collected during the Tropical Rainfall Measuring Mission to look at tropical cyclones and found that rainfall cycles found in the satellite data were similar to that found by observations by Gray and Jacobson (1977). Bowman and Fowler (2015) also found a 6 AM local time peak in rainfall in a composite of 85,000 observations of tropical cyclones. Wu and Ruan (2016) found that minima in IR brightness temperature in Typhoon Saola occurred prior to sunrise, due to nighttime radiative cooling (Melhauser and Zhang, 2014; Duran et al., 2021).

Dunion et al. (2014) studied TCs from 2001 to 2010 and found an outward pulse of cloud-top temperature related to behavior of the cirrus canopy, starting near the storm's center near sunrise. Ruppert and O'Neill (2019) attributed this pulsation as a response to solar warming, exciting inertia-gravity waves to travel outwards from the storm center, which work to then reduce the temperature anomalies. Navarro and Hakim (2016) hypothesized that solar

warming and latent heating were both important to aspects of the diurnal cycle of tropical cyclones.

Ruppert and Hohenegger (2018) found that the lapse-rate mechanism, which states that cooling overnight leads to greater convection, creates a bottom-heavy circulation, where convective heating is strongest in the lower troposphere, allowing for deeper convection. However, the differential cloudy-clear radiation mechanism delays the peak for about five hours, explaining differences in peaks of rainfall between their organized (closer to midnight) and unorganized (closer to 6 AM) convection model outputs. Evans and Nolan (2022) found a similar result in the height of the cirrus canopy. Results in Hitchman and Rowe (2024) show a similar pattern change from a peak at midnight to a peak at 6 AM when looking at UTLS σ_{PV} in mature hurricanes versus weaker hurricanes.

1.3. Why Potential Vorticity?

The ECMWF (2016) model provides Ertel's PV in pressure-coordinates, which ECMWF calculates from zonal, meridional, and vertical winds (u, v, and ω) and temperature (T) (ECMWF 2023). Although the ECMWF model does not use the conservation equation for Ertel's PV to calculate potential vorticity, this equation is useful for discussing formation mechanisms. Following Andrews et al. (1987), Ertel's PV is defined to be:

$$P = \frac{1}{\rho_o}\frac{\partial \theta}{\partial z}(f+\zeta) - \frac{1}{\rho_o}\frac{\partial \theta}{\partial x}\frac{\partial v}{\partial z} + \frac{1}{\rho_o}\frac{\partial \theta}{\partial y}\frac{\partial u}{\partial z} \qquad (1.1)$$

, with the potential vorticity conservation equation (1.2) obtained from their equation (3.1.5):

$$\frac{DP}{Dt} = \frac{1}{\rho_0}\left[\frac{\partial \theta}{\partial z}\left(\frac{\partial Y}{\partial x} - \frac{1}{cos\Phi}\frac{\partial (cos\Phi X)}{\partial y}\right) + \frac{\partial X}{\partial z}\frac{\partial \theta}{\partial y} - \frac{\partial Y}{\partial z}\frac{\partial \theta}{\partial x} + (f+\zeta)\frac{\partial Q}{\partial z} + \frac{\partial Q}{\partial y}\frac{\partial u}{\partial z} - \frac{\partial Q}{\partial x}\frac{\partial v}{\partial z}\right]. \qquad (1.2)$$

Where X and Y are the components of the net viscous force per unit mass, and Q is the diabatic heating rate for potential temperature, and θ is the potential temperature. PV anomalies are

created through diabatic processes. In the PV conservation equation, these processes are represented by the diabatic stretching tendency, $\frac{1}{\rho_0}(f+\zeta)\frac{\partial Q}{\partial z}$, and diabatic tilting tendency, $\frac{1}{\rho_0}(\frac{\partial Q}{\partial y}\frac{\partial u}{\partial z}-\frac{\partial Q}{\partial x}\frac{\partial v}{\partial z})$, and can be advected into the UTLS quickly by updrafts (Hitchman and Rowe 2024).

PV dipoles in the UTLS are created when an updraft brings horizontal winds to a layer with differing winds. Chagnon and Gray (2009) found that vertical wind shear was needed for these horizontal dipoles to be formed. Hitchman and Rowe (2014) found dipoles on the order of 10 PVU, similar to maximum values of σ_{PV} in this work. The inertially unstable member of the dipole (negative member in the Northern Hemisphere) is formed radially outward of the cyclonic jetlet in a TC (Hitchman and Rowe, 2019). This member of the dipole can play a role in enhancing downstream convection (Holland and Merrill, 1984).

1.4. Research Objectives

This thesis seeks to answer three main questions regarding UTLS potential vorticity variability observed in Gulf of Mexico tropical cyclones using ECMWF high resolution data.

1. Is the diurnal cycle of σ_{PV} (standard deviation of potential vorticity) in a mature hurricane (category 2 or stronger, or C2S) different than that in a weaker hurricane (category 1 or weaker, or C1W)? In particular, does the peak in σ_{PV} shift from 6 AM to midnight, as anticipated by Ruppert and Hohenegger (2018)?
2. Does σ_{PV} propagate radially outward over the course of a day, similar to the cycle in cirrus canopy found by Dunion et al. (2014)?
3. Does the diurnal cycle of σ_{PV} change when a storm nears landfall, similar to results found in Gray and Jacobson (1977) and Jiang et al. (2011)?

Chapter 2 describes the data sets and methods used in this research. In Chapter 3 a case study of the lifespan of Hurricane Marco will be presented, and the diurnal cycle will be assessed. Chapter 4 describes results from the composite analyses and discusses statistical significance of the findings. Lastly, Chapter 5 provides conclusions and a description of potential future work.

Chapter 2. Data Sets and Methods

2.1. PV Variability

This thesis investigates the temporal variation of potential vorticity (PV) in tropical cyclones (TCs), using a measure of mesoscale variability over the domain. σ_{PV}, or the root mean square of PV is calculated as $\sigma_{PV} = \sqrt{\overline{PV'^2}}$, as in Hitchman and Rowe (2024). These values are then expressed in potential vorticity units (PVU). Results in this paper are shown for the whole domain of the storm (666 km x 666 km) at every time-step, which is further divided into four quadrants of (333 km x 333 km) (Figure 2.1a), and rings of 111 km, 222 km, and 333 km radii (Figure 2.1b).

2.2. European Centre for Medium-Range Weather Forecasts IFS High-Resolution Operational Forecasts

This thesis uses data from the European Centre Medium-Range Weather Forecasts IFS High Resolution Operational Forecasts (ECMWF, 2016). These operational 6-hourly atmospheric isobaric analyses have a grid-point spacing of 0.07° or ~ 7.8 km. The data set is available from 1 January 2016 to the present day, which fully encompasses the time period of storms studied in this thesis. The main variable researched in this paper, potential vorticity, is calculated in the ECMWF model using wind, temperature, and pressure values (ECMWF, 2023). The National Center for Atmospheric Research Data Support Section (NCAR) transformed the ECMWF data set into a 5120 longitude by 2560 latitude Gaussian grid.

ECMWF data are downloaded for each 6-hour time interval encompassing the whole storm duration. At each timestep, a subset of 86×86 grid points is extracted in an array centered on the storm track, which is defined by the National Hurricane Center's Best Track data

(HURDAT, short for Hurricane Databases). Each 86 x 86 grid is further binned into quadrants and annuli, which will be defined in sections 2.4 and 2.5.

2.3. National Hurricane Center Reports and Best-Track Data

For every time step over the course of a storm, the center is determined using the National Hurricane Center's (NHC's) Tropical Cyclone Reports that were released for each storm months after the storm occurred. Each of these reports give detailed descriptions of the intensity of the storms, the history of their formation, and statistics of damage, casualties, warnings, and watches that were generated over the lifespan of the storm. These reports also include the best track estimate for the center of the hurricanes at each timestep. The same timeline is found using NHC's HurDat data set, which is used to specify the storm track center locations. The HurDat data set contains estimated storm tracks dating back to the 1800s. The data set also includes minimum sea level pressure and maximum wind speed observed near the center of the storm. Using the HurDat's maximum wind speed values, the intensity of the storm is classified according to Table 1.1. The HurDat timeline matches the timeline of the ECMWF dataset used, thus the NHC best track estimate is used as the center of the storm when extracting the subset of data from the ECMWF grid.

2.4. Quadrant Method

The HurDat's best track data set allows for our original binning of the NCAR ECMWF grid around the center latitude and longitude. Originally, an 86 x 86 grid is created around the best track center, and this represents the entire domain of the storm, approximately a 666 × 666 km square. The entire domain is then binned once again into four quadrants that were labeled

based off their orientation in the storm. Figure 2.1a depicts where each quadrant lies in relation to the center of the storm (Hitchman and Rowe, 2024).

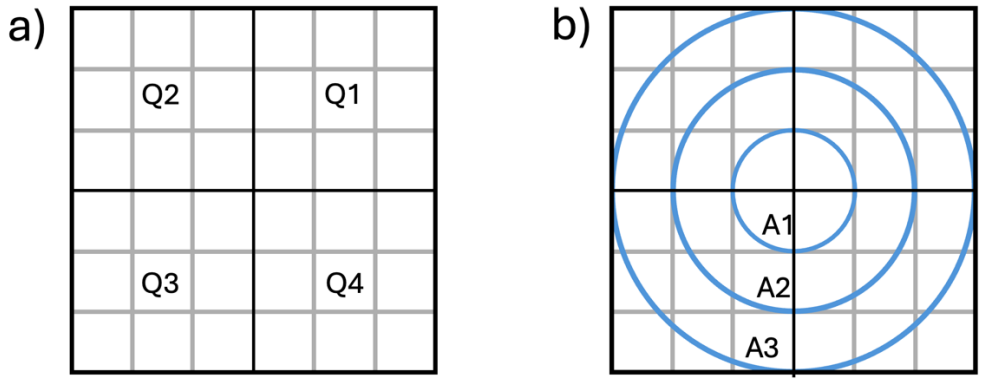

Figure 2.1. a) Depiction of whole storm domain broken into four quadrants. Naming convention always has Quadrant 1 in the northeast corner of the storm, and then naming progresses counterclockwise. b) Depiction of annulus method, with A1 representing the inner ring, A2 representing the middle ring, and A3 representing the outer ring.

From Figure 2.1a, we see that Quadrant 1 is the northeast quadrant of the storm. Numerically the quadrants progress counterclockwise, where Quadrant 2 is the northwest quadrant, Quadrant 3 is the southwest quadrant, and Quadrant 4 is the southeast quadrant. The figure also shows the size of each quadrant. Since the entire domain of the storm is an 86 x 86 grid, each quadrant then is 43 x 43 grid points, or ~ 333 × 333 km in area. Each quadrant holds 1849 data points, and the whole domain is 7396 data points.

The Quadrant method is useful for looking at the progression of σ_{PV} in different regions of the storm. Mesoscale variability in σ_{PV} can be analyzed due to the structure of updrafts in the cyclone. A couple of features that can lead to local asymmetries are land coverage (the percentage of surface in each subdomain over land), and wind shear. The additional binning can also allow for patterns to be shown which may be flattened out when averaging over the entire 86 x 86 grid box.

2.5. Annulus Method

The annulus method is used to determine if there is a noticeable radial propagation of σ_{PV} outward from the center over the course of a day. Binning is similar to that of the additional binning for the quadrant method. However, instead of being divided into four quadrants, the original domain is broken into three rings of different diameters around the center of the storm given by HurDat. Figure 2.1b shows pictorially how these rings look from an overhead view of the storm. The first ring has a radius of 111 kilometers, centered at the storms center. Ring 2 has a radius of 222 kilometers around the center of the storm; however, the inner circle of 111 km radius is removed, isolating the part of the ring which does not overlap with the first ring. Ring 3 is similar in nature, where it has a radius of 333 km, but the inner circle of 222 km is removed to again isolate the ring.

2.6. Statistical Tests Performed

Two main statistical significance tests were used when evaluating the data; the Welch's t-test and the Analysis of Variance (ANOVA) test.

2.6.1. Welch's t-test

The Student t-test (Student, 1908) is a statistical test that assesses whether or not the means of two data groups are statistically different (Mishra et al., 2019). The resulting p-value of the test tells the user if the means are significantly different from each other (p-value small) or if there is no real difference between the means (p-value large). In the work that follows, a one-sided Welch's t-test (West, 2021; Welch, 1938) was used to determine if data divided into

different time bins differed in distribution. The t-tests are conducted after an Analysis of Variance test to conclude that at least one bin had a significantly different mean than the other time bins.

The reason for using a Welch's T-test versus a Student T-test is due to differences in variance. A Student's T-test assumes that the variance of both groups are equal. However, when using a Levene test (Mishra et al., 2019) to check for equal variance between bins, the results showed that some, but not all, data bins had an equal variance. Also, the sample sizes in each of the bins are not equal. The combination of non-equal sample sizes and a difference in variances led to the decision to use Welch's t-test. Lastly, it has been shown that using Welch's t-test on data with equal variance leads to conclusions similar to those of a Student's t-test (West, 2021).

2.6.2. Analysis of Variance test (ANOVA)

An Analysis of variance (ANOVA) test was used to test the means of each of the time bins against each other when binning data. An ANOVA test compares the means of multiple groups and shows if there is one group-mean which is different than another (Mishra et al., 2019). If there is one such mean that is drastically different than another group's mean, then the ANOVA test will return a small, statistically significant p-value (Mishra et al., 2019). The ANOVA tests used in this thesis were done prior to performing a Welch's t-test or a Mann-Whitney U-test.

2.7. Times Used

The data were originally provided in Coordinated Universal Time (UTC) for ECMWF variables and the storm track. This was then converted to the local time for each time step using

proper time zones based on where storms were positioned at each time step. Times were converted to daylight saving time for time steps that fell between March 8 and November 1, 2020. Any time steps that fell after November 1 at 2 AM local daylight time were converted to standard time (most of Hurricane Eta and all of Hurricane Iota). All storms in 2021 and 2022 were converted to daylight saving time.

Chapter 3. Hurricane Marco Case Study

3.1. Introduction to storm

Hurricane Marco was the 13th named storm of the Atlantic Hurricane season, and the third storm system to cross through the Gulf of Mexico. Marco impacted multiple areas, including Cuba, Central America, and the Gulf Coast of the United States. Although Marco was not a particularly damaging storm, the timing of it along the Gulf Coast was significant, as major hurricane Laura made landfall close by, shortly after Marco dissipated.

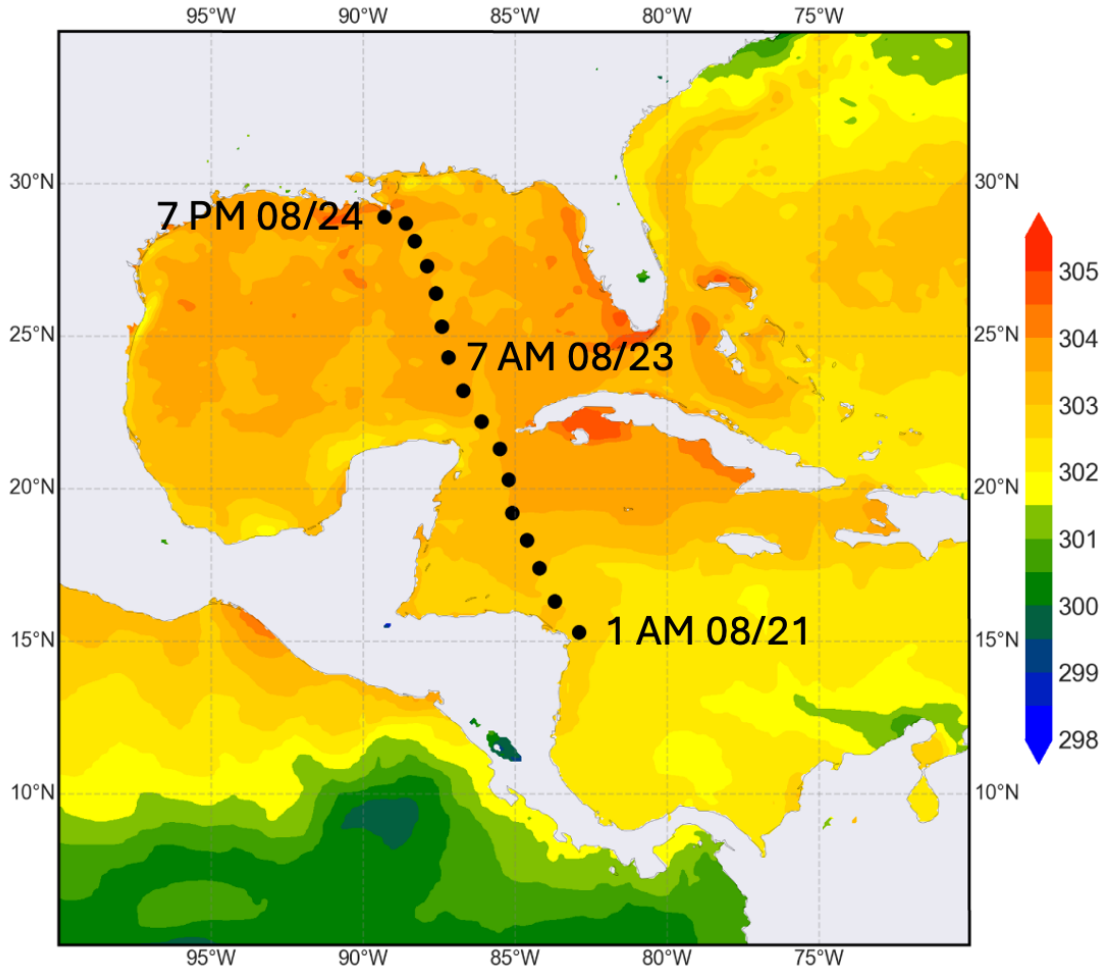

Figure 3.1. Hurricane Marco sea surface temperature plot with hurricane track (HURDAT) overlayed. Three key times are highlighted, when Marco first organized into a TD, when Marco first intensified to C1, and the last time-step before Marco dissipated.

Hurricane Marco was a short-lived TC which traversed through the Gulf of Mexico in August of 2020. The storm system began as a tropical wave off the coast of Africa which formed 10 days before Marco was first classified as a TD (Bevin and Berg, 2021). Marco never made official landfall, however. Both when first strengthening near Central America (1 AM August 21, Fig. 3.1), and when dissipating near Louisiana (7 PM August 24, Fig. 3.1), the center of the storm was very close to land (Bevin and Berg, 2021). Figure 3.1 suggests how Marco was aided by favorable sea surface temperatures (SSTs) in the Gulf of Mexico, where temperatures were 302 K (28.85°C) or warmer. Marco strengthened to C1, with maximum wind speeds of 65 kt during the morning of August 23 (Fig. 3.1) before weakening to a TS that afternoon due to wind shear (Bevin and Berg 2021). As the storm moved closer to the Gulf Coast, it continued to weaken before dissipating, with the center of the storm being located just off the coast of Louisiana.

Figure 3.2a shows 250 hPa geopotential height on the morning of August 23, 2020, when Marco intensified to C1. A noticeable upper-level trough is present over Texas and Mexico, to the northwest of Hurricane Marco. Over the course of Hurricane Marco's duration, this trough steered Marco toward the north-northwest (Bevin and Berg, 2021). The trough played a major role in keeping Marco from ever making landfall, as it steered the storm center off the coasts of Central America and Cuba early in the storm's lifespan. It also created wind shear that caused Marco to dissipate off the coast of Louisiana (Bevin and Berg, 2021). Figure 3.2b shows 700 hPa geopotential height at the same time as Fig. 3.2a. In this, Marco has entered the Gulf of Mexico, having passed Cuba and the Yucatan Peninsula. Behind Marco, Hurricane Laura is starting to deepen in the Caribbean (Fig.3.1b). Hurricane Laura would follow a similar path to Marco, becoming the first major hurricane of the 2020 Atlantic hurricane season.

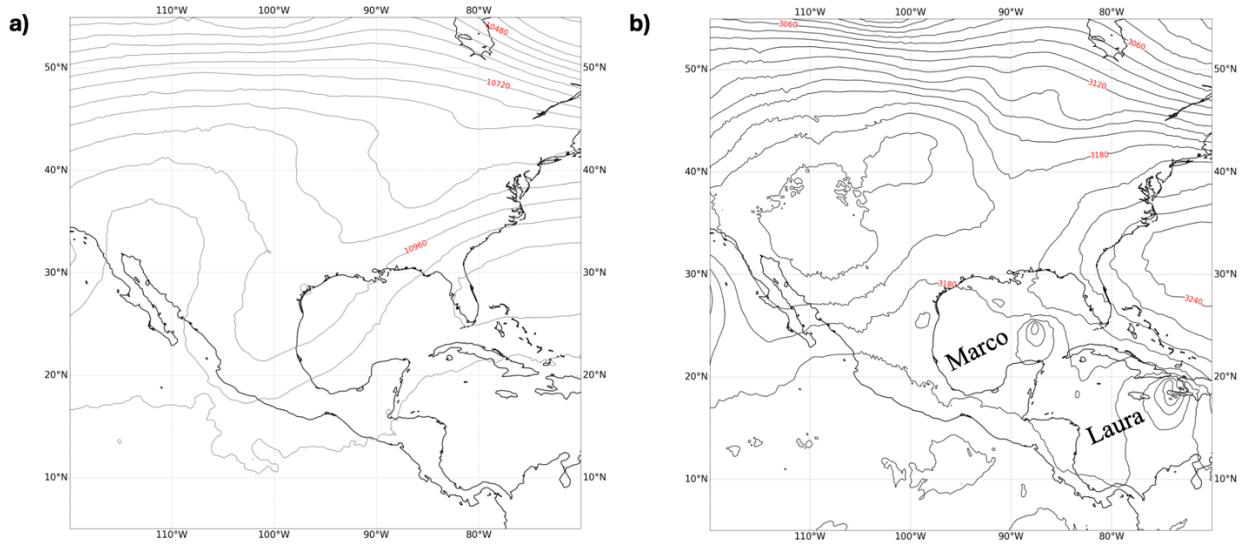

Figure 3.2. a) 250 hPa geopotential height (m) and b) 700 hPa geopotential height (m) on the morning (give time) of August 23, 2020.

3.2. Diurnal cycle in PV variability

3.2.1 Whole Storm Domain

It is hypothesized that the diurnal cycle of σ_{PV} in Hurricane Marco would have maxima and minima that would align with prior research focused on the convection and rainfall diurnal cycles in TCs. For Hurricane Marco, past research would suggest maxima in σ_{PV} found near sunrise and minima in the late afternoon/evening (Jiang et al., 2011, Ruppert and Hohenegger, 2018), as Marco never intensified past C1. It is also important to note that, for the duration of when Hurricane Marco was first classified as a TD up until when it dissipated, the hurricane never made landfall. Since Marco never made landfall, it is not expected that there would be a second maxima in σ_{PV} found in the afternoon similar to convection in Jiang et al. (2011) and Gray and Jacobson (1977). Figure 3.3 shows that σ_{PV} at 100 hPa in Hurricane Marco over the

whole storm domain exhibits a peak around sunrise (7 AM) for two of the three days when Marco was classified as a TS or stronger. The third day of Marco's lifespan showed a slightly later peak around 1 PM. Daily minima in σ_{PV} occurred in the later evening of each day, around 7 PM local time. These maxima and minima align well with the previously stated hypothesis.

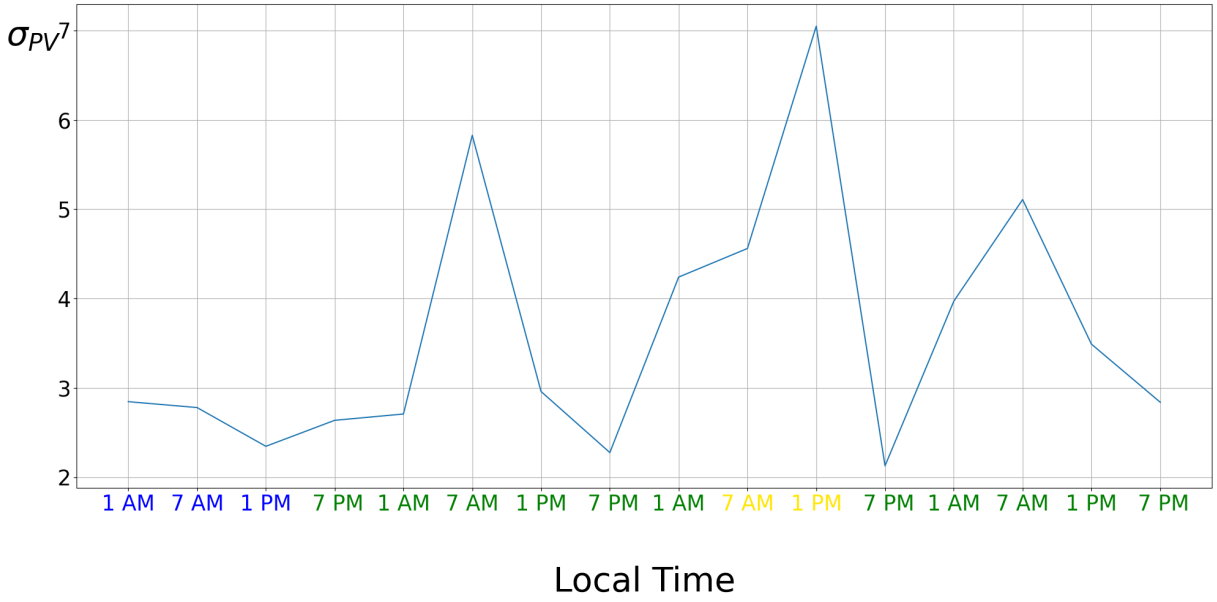

Figure 3.3. Time series of ECMWF 100 hPa σ_{PV} for TC Marco during 1 AM August 21 to 7 PM August 24 CDT, using the full storm domain.

Figure 3.4 shows the distribution of σ_{PV} in four time bins, which includes data from 1 AM August 21 – 7 PM August 24 CDT. This binning presents a complementary view of the diurnal cycle found in Hurricane Marco. Each "violin plot" shows the density of data points as proportional to width. A wider portion of the violin plot means that there are more samples with that value of the vertical axis. Thin regions indicate little to no data points. If we were to look at the violin plot representing 1 AM Local Time for Marco, there are two regions that are similarly wide. Each of these regions have two data points in the vicinity. The thin portion in the middle shows that there are no data points in the middle of the distribution. So, there is a bimodal

distribution. Inside of each violin diagram is a thin black line and a thick black line. The thin black line spans the violin and shows the range between the maximum and minimum values. The thick black line shows the interquartile range (75th percentile – 25th percentile). The black lines are not important when looking at Hurricane Marco due to lack of data, however, they are when looking at composite results in Chapter 4. Looking at Fig. 3.4, a peak in σ_{PV} is seen around 7 AM, where there are multiple data points (3) in between 4 and 6 PVU. The 1 PM violin plot shows the early afternoon maximum which is seen in Fig. 3.3. However, the 1 PM violin plot is widest around 2.5 – 3.5 PVU.

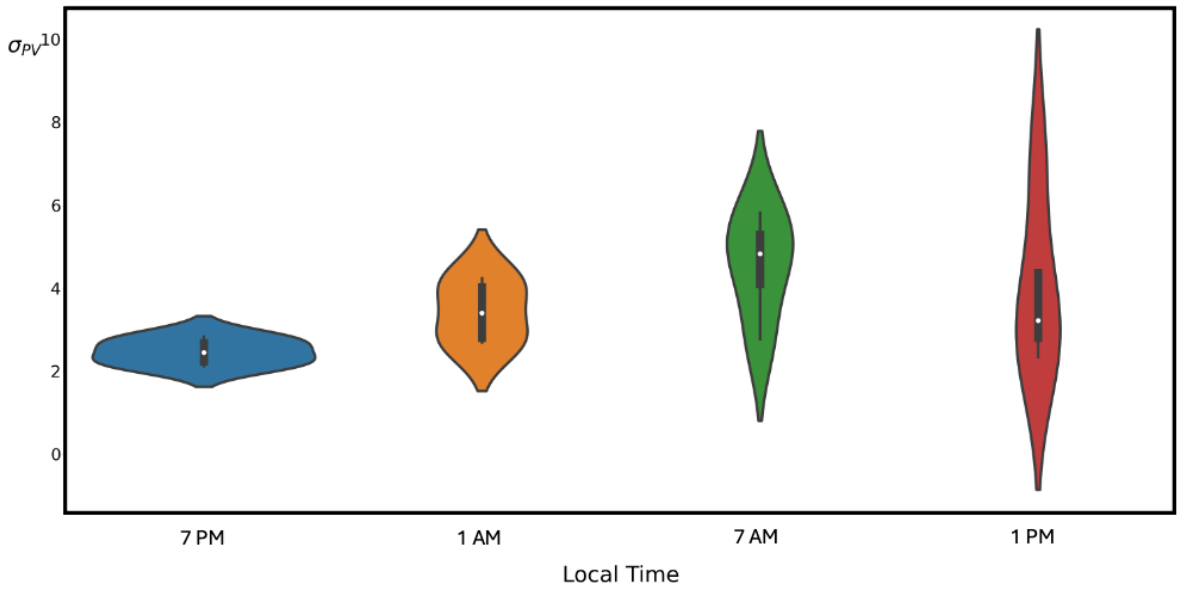

Figure 3.4. Distribution of values of 100 hPa σ_{PV}, or "violin plot", used in ANOVA test for TC Marco for the whole storm domain during 1 AM August 21 to 7 PM August 24, 2020 CDT.

The spatial and temporal correlation between stronger PV dipoles and convective strength can be seen in Fig. 3.5. Here, the diurnal cycle of both PV at 100 hPa and the channel 13 clean IR window satellite are shown. The clean IR window is chosen as it can be used to estimate cloud top brightness temperature (CIMSS).

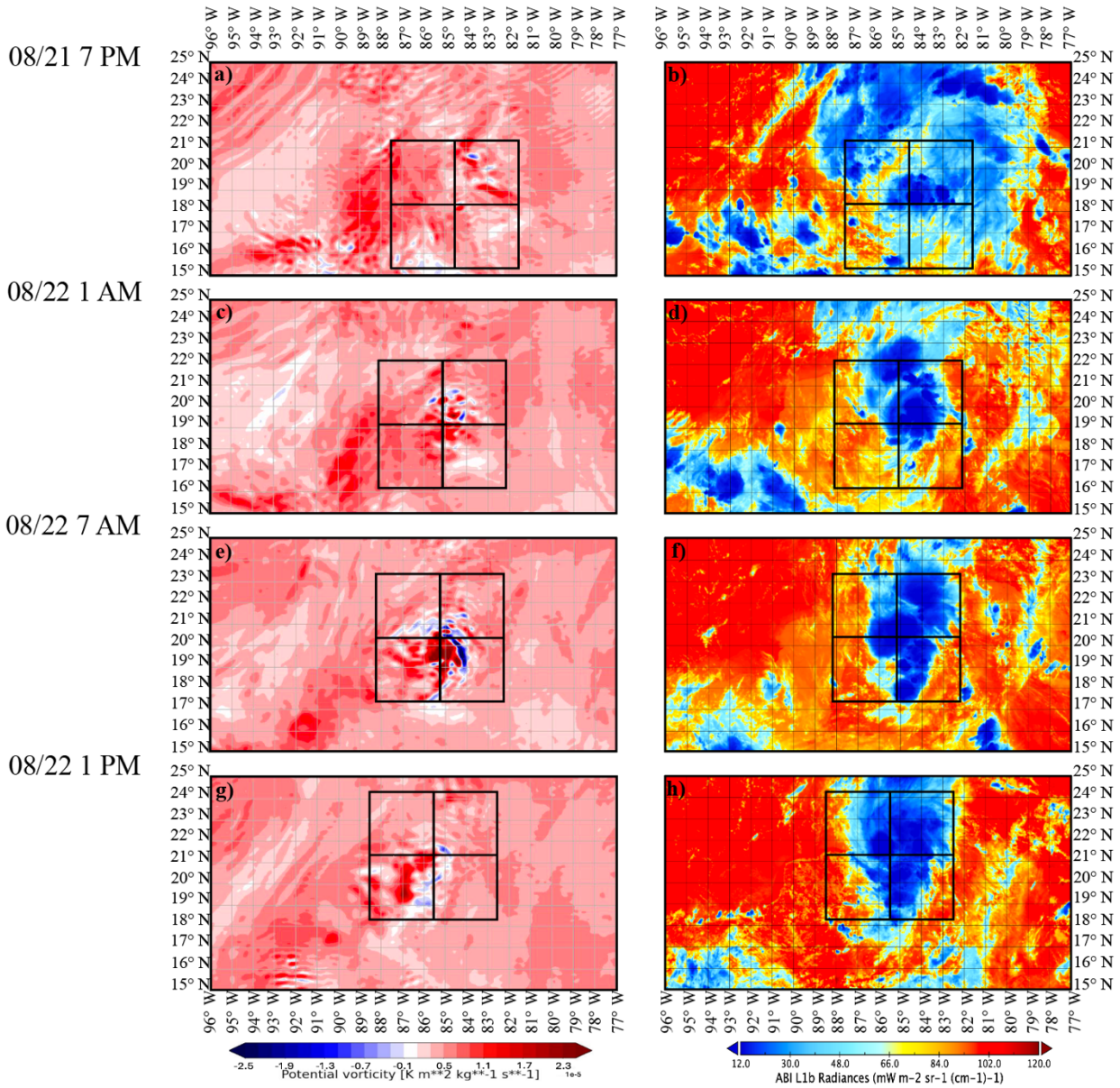

Figure 3.5. Maps of 100 hPa potential vorticity (left), and Channel 13 IR longwave outgoing radiances (right), showing the correlation between PV characteristics and convection throughout the course of one day (7 PM CDT 21 August, 1 AM CDT 22 August, 7 AM CDT 22 August, and 1 PM 22 August) over Hurricane Marco.

In the PV maps on the left, a clear diurnal cycle in PV dipoles is seen. A peak in strength of dipoles can be seen at 7 AM, August 22 (cf. Fig. 3.3). This peak aligns with strong minima found in the IR radiances on the right. These minima suggest strong convection in this area. A feature to notice is that both the PV filaments and the convection have a similar comma shape. In Quadrant 1, extended convection is found radially outwards from the negative PV filament (inertially unstable).

3.2.2 Quadrant Method

σ_{PV} in each of the four quadrants of TC Marco has the same pattern as σ_{PV} for the whole storm domain. There were some minute differences both between the whole storm σ_{PV} and individual quadrants, and σ_{PV} between two separate individual quadrants. As stated above, Marco was closest to land, both as it was first strengthening to a TD near Central America, and then as it started to dissipate off the Louisiana coast. Due to this positioning, we hypothesized that certain quadrants may peak at different times, depending on if they were over land or not, following Gray and Jacobson (1977) and Jiang et al. (2011).

Figure 3.6 shows that for the most part, each of the quadrants in TC Marco are peaking at the same time. σ_{PV} in quadrants one (northwest) and three (southeast) peak at the same time as the peak found in section 3.2.1 for the whole storm domain. Quadrant two (northeast) peaks in sync with these two quadrants on days two through four, and quadrant four (southwest) does not peak in sync with the other quadrants on days 1 and 3. Although this difference was not explored further in this case study, it provides a hypothesis which will be tested in the composite analysis. The hypothesis is that land could have an important effect on the diurnal cycle for quadrant four. On the first day, when Hurricane Marco was first classified as a Tropical

Depression, both quadrants two and three were partially over Central America. Considering how winds around the center of a TC rotate in the Northern Hemisphere, this means that quadrant four would be receiving dry air from the continent, compared to the moist air that quadrants one and two would be getting.

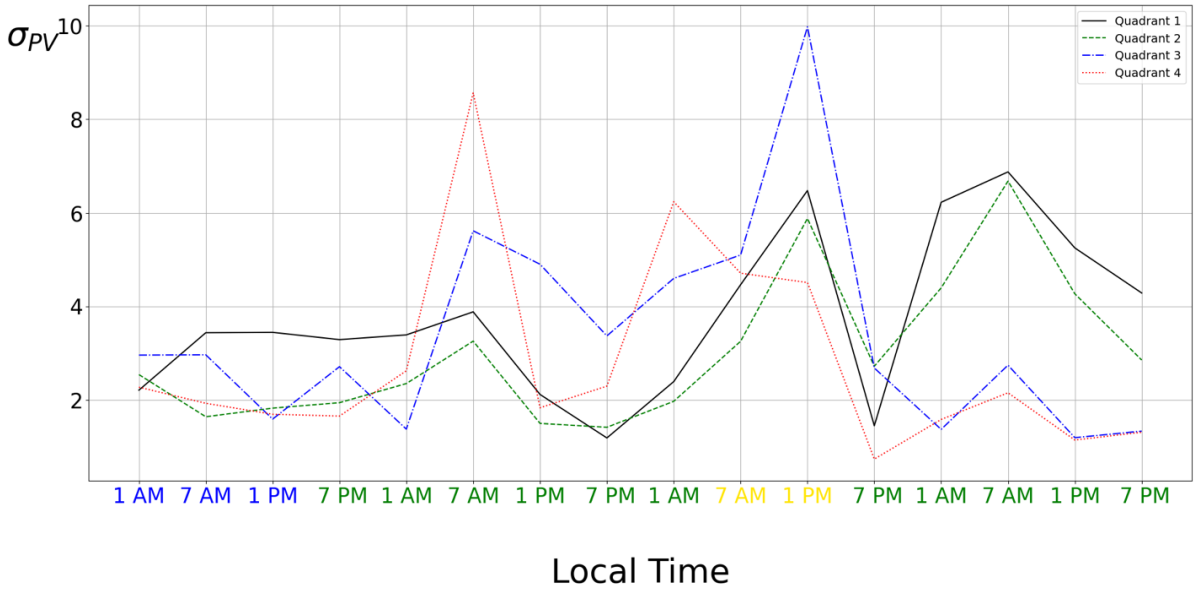

Figure 3.6. Time series showing σ_{PV} for each of TC Marco's quadrants. Quadrants were made to determine if the diurnal cycle of σ_{PV} differs in different sections of the storm.

3.2.3 Annulus Method

The annulus method is used to see if maxima in σ_{PV} propagate outward like Dunion et al.'s (2014) results observing the cirrus canopy of TCs. Dunion et al. (2014) found that, over the course of a day, the timing of the peak in higher clouds varied with radius away from the storm center. Using IR brightness temperature, the authors found that the cirrus canopy propagated outward from the center of the storm from early morning to sunset. Then, the cirrus canopy would shrink again until starting the process over again the next morning (Dunion et al 2014).

This led to the creation of an annulus method for this thesis. It was hypothesized that σ_{PV} should not propagate outwards like Dunion et al's work, since σ_{PV} is tied to the location of the updrafts instead of to the outflow cirrus. The strongest updrafts found within a TC is near the center of the storm, and the PV dipoles which σ_{PV} measures are formed due to those.

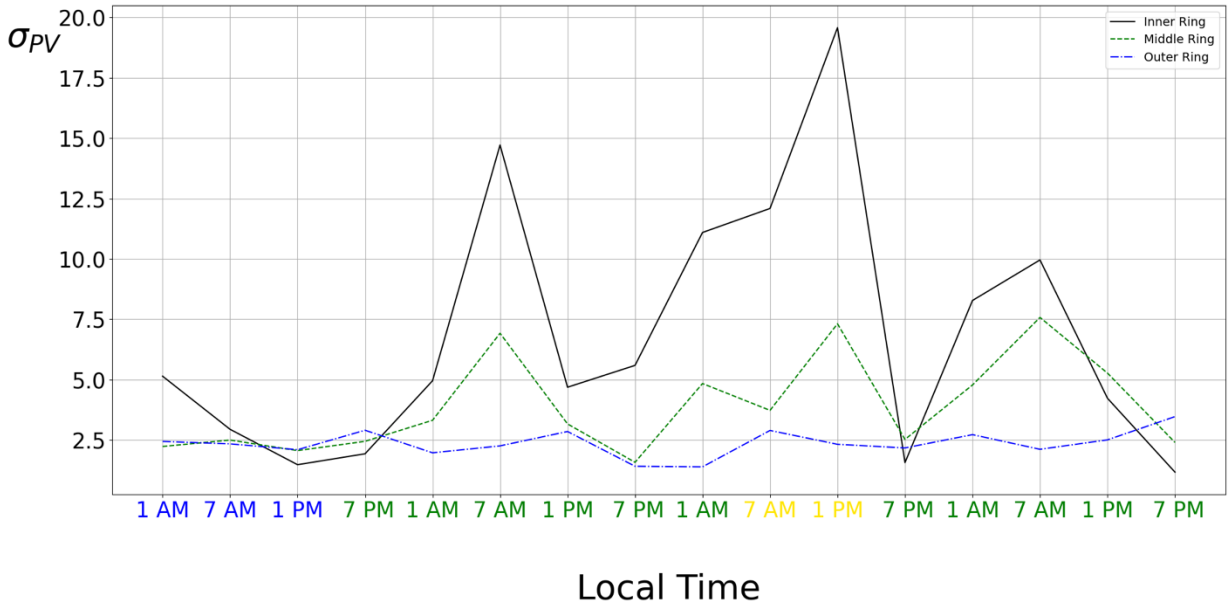

Figure 3.7. Time series showing σ_{PV} for each of TC Marco's annuli. Annuli were made to determine if σ_{PV} propagates outwards similar to Dunion et al's (2014) work with the cirrus canopy.

In Fig. 3.7 there is no pattern that hints of outward propagation of σ_{PV} over the course of a day. The inner ring of Hurricane Marco shows peaks at the same interval as the whole storm domain, and has larger σ_{PV} values than the middle and outer rings for the majority of the storm. The middle ring seems to peak in synchronicity with the inner ring, and again has higher values of σ_{PV} than the outer ring for much of the storm. These features are important to note, as a large value of σ_{PV} would correlate with stronger convection, and the strongest convection should be found towards the center of the storm. The outer ring does not peak in synchronicity with the

inner and middle rings. It has a much different pattern over the course of the storm, peaking at a different time each day. The unorganized nature of these peaks shows that there is little to no diurnal cycle in convection along the outskirts of TC Marco.

3.3. Chapter Summary

Hurricane Marco exhibits a noticeable diurnal cycle in σ_{PV} at 100 hPa. Marco was short-lived (four days from first being classified as a tropical depression to ultimate dissipation), thus no significance testing was done. However, Figs. 3.3 – 3.7 show a pattern of larger σ_{PV} values in the morning, with minima found in the late evening. Over most of Marco's duration, σ_{PV} in all four quadrants peaked at the same time each day, with small discrepancies which can be due to quadrants being partially over land. The annulus method shows no pattern hinting at outward propagation. Instead, σ_{PV} in the middle and outer rings seem to peak at the same time as each other. The peaks for these two rings follow the peaks found over the whole storm. The outer ring seems to peak at varying times over the four days and does not show a pattern that alludes to a preference of time for these peaks.

Due to Marco being short-lived, the effects of land on the diurnal cycle are not looked at in detail. Overall, there was not enough data to make strong conclusions regarding whether the diurnal cycle did indeed change when certain quadrants were partly over land. This will be examined further when looking at composite results, along with more solid statistical evidence looking at the diurnal cycle. Overall, Marco did show signs that our hypothesis has merit and led to the creation of the composite results shown in the next section.

Chapter 4. Composite Results for 2020 and for 2020-2022 Gulf TCs

4.1. Description of composites

After researching each of the 2020 hurricanes individually, a composite was made to test the validity of results. By combining the storms into one data set, observations that were seen in individual storms could be tested statistically. This allowed for binning by strength of storm and by percentage of storm over land. Compositing allows for statistical testing, as the sample sizes are greater than for an individual storm. It was hypothesized (Question 1) that when the composite data is binned by storm strength, the timing of the peak of σ_{PV} would differ. The subset of storm days where storms were C2 or stronger is expected to have a peak in σ_{PV} near midnight, while the subset of storm days where storms were C1 or weaker is expected to have a peak near 6 am. This result would be consistent with the results of Ruppert and Hohenegger (2018), if true. It was also hypothesized (Question 3) that land would influence the diurnal cycle of σ_{PV}. It is expected that the diurnal cycle of σ_{PV} as a storm progressed farther over land would mirror results in rainfall and convection found in Jiang et al. (2011), and Gray and Jacobson (1977), where a second, greater peak would be found in the afternoon.

Two composites were made. The first was a composite of just 2020 Gulf of Mexico hurricanes. This was the subset of storms used when beginning research on this subject and consists of the storms listed in Table 1.2. However, when binning by storm strength, there still was a relative lack of sample size, so a second composite was created. This composite included Gulf of Mexico storms from 2020 through 2022. Six storms, four from 2021 and two from 2022, were added to the original composite (Table 1.3), resulting in a total of 15 storms in the second composite.

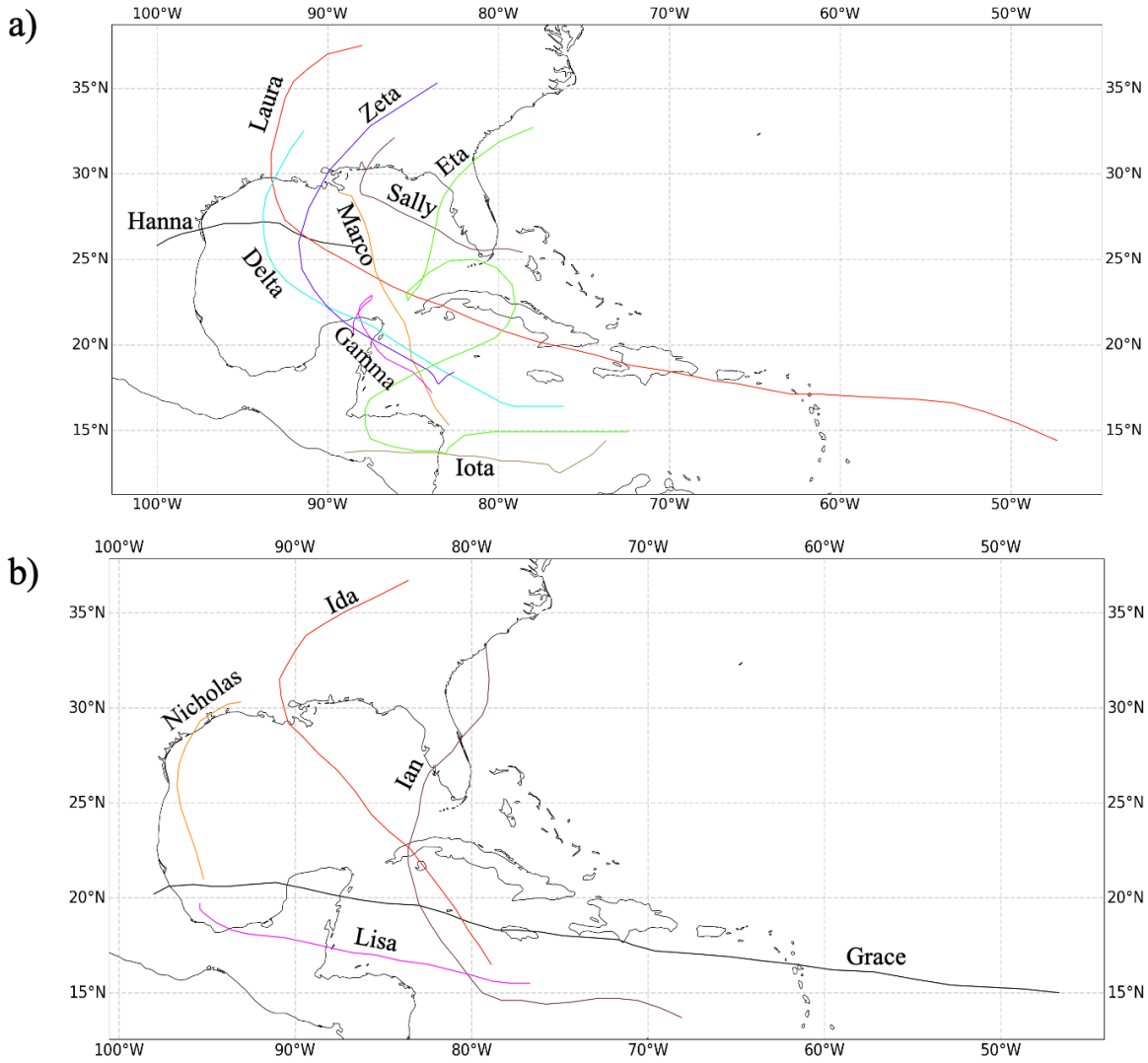

Figure 4.1. Hurricane tracks for the a) 2020 TC composite and b) for the additional 2021 and 2022 TCs used in the 2020 - 2022 composite.

Each composite data set was first binned by storm strength. Two subsets were created, one being category 1 or weaker (C1W) storms, where all data were taken from times when each storm was classified as C1W according to the Saffir-Simpson scale, and the other being category 2 or stronger storms (C2S). The C1W subset had much more data in it than the C2S subset, partially since not every storm in each composite reached strength C2. The discrepancy in sample size between the two subsets led to the addition of six more storms from 2021 and 2022 to include in the second composite.

Later, the composite data sets were also binned by fraction of storm over a land mass. The ECMWF land mask variable was used to assign each grid box in the model a number between zero and one, which represents the percentage of the box over land. A land mask of zero means that a box is fully over water, whereas a land mask of one means that the grid box is fully over land. Any number between zero and one represents a grid box that is partially over land and water. Since the whole storm domain consisted of 86×86 grid boxes, a percentage can be calculated for how much of a storm was over land for each given time step. For example, if a storm were fully over land for a specific time step, the land mask total would be 7396, and if the storm were only half over land, the land mask would be 3698. Not only can the land mask be used to evaluate the entire storm domain, it can also be easily used to look at different quadrants, which may be helpful in understanding why certain quadrants do not always have the same diurnal cycle as others.

4.2. Whole Storm Domain

4.2.1. Category 1 or Weaker Storms

4.2.1.1. Results for 2020 Composite

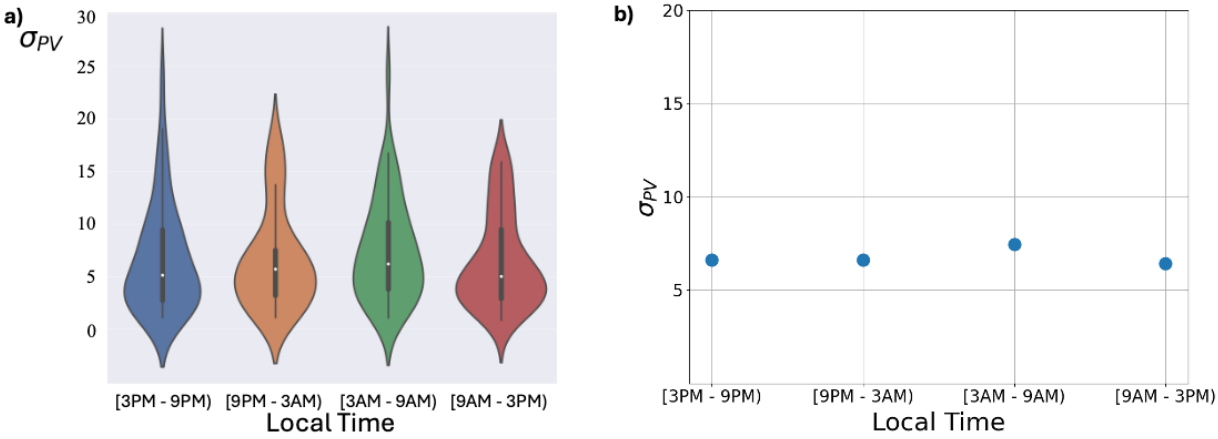

Figure 4.2. a) Violin plots showing the distributions for each time bin (in PVU) for the 2020 C1W composite. Wider portions of violins mean higher density of data points. b) Mean values of σ_{PV} for each local time bin.

As in the Hurricane Marco case study above, the full domain was used for analyzing the diurnal cycle. When binning into the four time bins, each bin for the 2020 composite had N = 48. Figure 4.2a shows how the values were distributed between the four time bins for C1W in 2020. Each time bin will be referred to as the middle time held within the bin (i.e. the [9PM – 3AM) bin will be referred to as the 12 AM or midnight bin). In comparison to the violin plot shown in the Hurricane Marco case study, the distributions for each bin in Fig. 4.2 do not vary drastically. Also, it should be noted that the thin black line in each violin shows the range of the data in each bin. The more solid black line shows the interquartile range. Since Hurricane Marco's bins only held four data points, these lines did not help me understand the distribution. However, since much more data is in each of these composite violin plots, the ranges should be noted. Here, in Figure 4.2, the widest portion of the 6 AM violin seems to be higher than the

widest portions of each of the other bins. This would suggest that there is a slight peak in σ_{PV} in the early morning hours around sunrise in C1W storms. This peak is slightly more noticeable looking at the plot of the time bin means in Figure 4.2b. However, the peak does not seem to largely differ from the other means , so this suggests that this peak is not statistically significant. When looking at the medians (white dots in each violin), the 6 AM peak becomes clearer, with median value 6.2 PVU. The median values for the 12 AM, 12 PM, and 6 PM time bins are 5.7, 5.0, and 5.1 PVU respectively. Thus, the peak of σ_{PV} does seem to be found in the 6 AM bin when looking at the distribution without using any statistics. This peak would be in line with the previous research done by Ruppert and Hohenegger (2018) who found that in an idealized model, rainfall peaked near sunrise in lesser organized storms.

Hypothesized Greater Time-bin	Hypothesized Lesser Time-bin	Welch's t-test p-value returned
[3 AM – 9 AM) *(6 AM)*	[9 PM – 3 AM) *(12 AM)*	.192
[3 AM – 9 AM) *(6 AM)*	[9 AM – 3 PM) *(12 PM)*	.135
[3 AM – 9 AM) *(6 AM)*	[3 PM – 9 PM) *(6 PM)*	.207

Table 4.1. Welch's one-sided t-test results for 2020 C1W.

To test if this 6 AM peak seen in Fig 4.2. is significant, a one-sided ANOVA test, and one-sided Welch's t-tests are performed. Since it is hypothesized that the peak in σ_{PV} is found at 6 AM, both due to previous cited research on the diurnal cycle of tropical cyclones, and from looking at Fig. 4.2, the one-sided t-test allows us to see if the mean of σ_{PV} in the 6 AM bin is greater than the mean of the other bins. The ANOVA test has a p-value of 0.712, suggesting that the null-hypothesis that the means of the four time bins are the same cannot be rejected. This result matches with the results of the t-tests performed shown in Table 4.1, where the p-values returned from the t-tests are not significant on a 0.1 or lower alpha level. However, since each of the p-values are small (~ 0.2 or less), they do suggest that there is a slight peak seen in σ_{PV} around sunrise.

4.2.1.2. 2020 - 2022 Composite

After statistically analyzing the 2020 composite, six new storms were added from 2021 and 2022 to form the 2020 – 2022 composite. Figure 4.3 shows the distribution of the 2020 – 2022 composite data. Although more data are now included in each bin (N = 83, 83, 81, 80), the plot has the same main features of the 2020 composite in the previous subsection. Overall, when adding the two years of extra data, the diurnal cycle is still not large. A peak in σ_{PV} in the early morning is slightly more noticeable when looking at the distribution of violins for each time bin. The means of each time bin (Fig. 4.3b) also show a discernable diurnal cycle, with a peak in the 6 AM bin of 6.2 PVU, and a slight minimum in the 12 PM bin of 5.0 PVU.

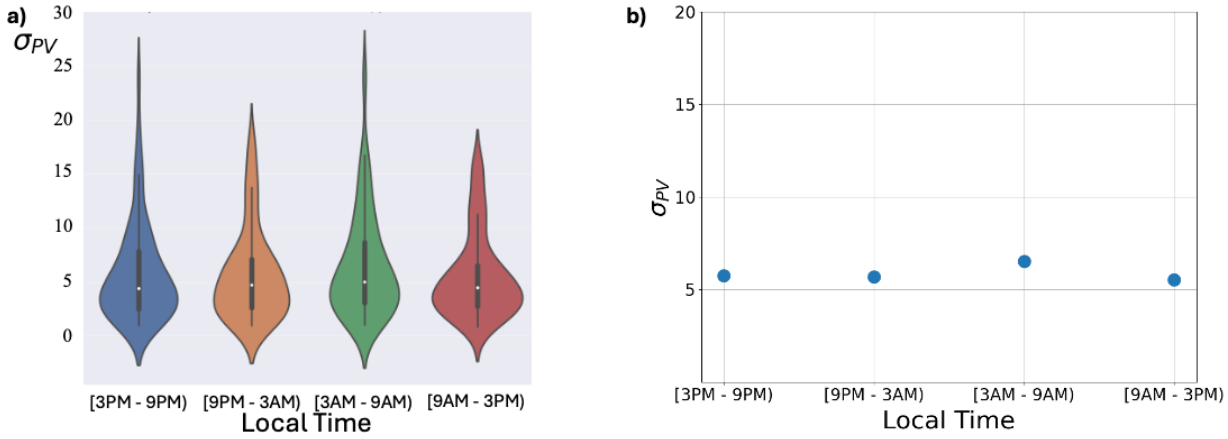

Figure 4.3. Violin plot showing distribution of time bins for the 2020 – 2022 C1W composite. b) mean of σ_{PV} for each time bin.

The results of the Welch's one-sided t-tests (Table 4.2), and ANOVA test performed on this composite show similar results to those found in the 2020 composite. For the 2020 – 2022 composite, the mean of the 6 AM time bin is not significantly different than the 12 AM bin and the 6 PM bin (p-value not below 0.1). However, it is significantly different than the 12 PM bin.

Although the p-values when comparing the 6 AM bin to the 12 AM and 6 PM are not significant, they still do suggest that there is a slight peak in σ_{PV} found near 6 am.

Hypothesized Greater Time-bin	Hypothesized Lesser Time-bin	Welch's t-test p-value returned
[3 AM – 9 AM) *(6 AM)*	[9 PM – 3 AM) *(12 AM)*	.125
[3 AM – 9 AM) *(6 AM)*	[9 AM – 3 PM) *(12 PM)*	.073 *
[3 AM – 9 AM) *(6 AM)*	[3 PM – 9 PM) *(6 PM)*	.147

* = significant on .1 alpha level

Table 4.2. Welch's one-sided t-test results for 2020 – 2022 C1W.

Although not statistically significant, results for the C1W composites do show a similar peak to the peak in rainfall found by Ruppert and Hohenegger (2018), using their idealized models for lesser organized storms. These results also are similar to peaks found in both Gray and Jacobson (1977) and Jiang et al. (2011), where each found a morning peak in rainfall and convection.

4.2.2. Category 2 or Stronger Storms

C2S was studied next to compare with the results of C1W. It was hypothesized that C2S would show a peak in σ_{PV} close to midnight, compared to the slight peak around 6 AM in C1W (Ruppert and Hohenegger, 2018).

4.2.2.1. 2020 Composite

A more pronounced diurnal cycle is seen when looking at the 2020 C2S, compared to both C1W composites. This is evident from Fig. 4.4, where a slight peak is seen in the midnight time-bin, and a noticeable minimum is seen in the late afternoon, and early evening. When looking at the medians of the data in each time bin, the peak in σ_{PV} around midnight (14.7 PVU)

becomes more noticeable. The smallest median value is found in the 6 PM time-bin (7.7 PVU).

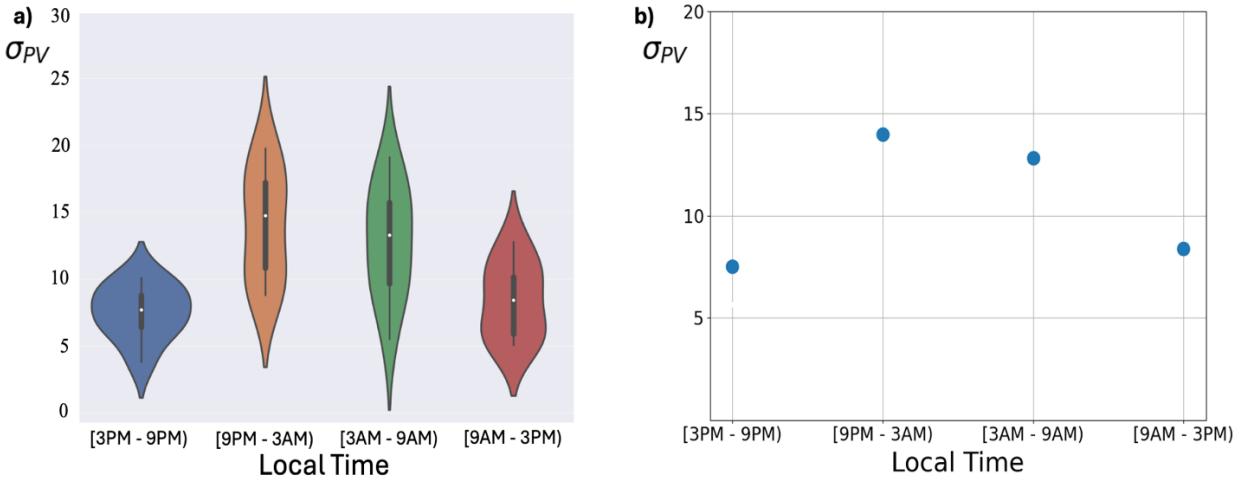

Figure 4.4. Violin plot showing distribution of 2020 C2S broken into four time bins. b) mean of σ_{PV} for each time bin.

Unlike the Welch's one-sided t-tests performed on the C1W subsets, the 12 AM time-bin is now hypothesized to hold the peak in σ_{PV}. This peak is noticeable when looking at Fig. 4.4b where the mean of σ_{PV} in the midnight bin is 14.0 PVU. Thus, each test will assume that the mean of the 12 AM bin is greatest, and test each other bin against this hypothesis. Results of an ANOVA test taken on the 2020 C2S data returns a significant p-value (0.0009), meaning that at least two of the time bins have means that are significantly different from each other. Table 4.3 shows results of each of these new Welch's t-tests. Overall, the mean of the midnight time bin is significantly greater than the mean of the noon time and 6 PM means, with p-values of 0.0029 and 0.0007 respectively. The p-value when comparing the midnight and 6 AM bin was not statistically significant (0.278), thus rejecting the null hypothesis that the midnight bin's mean is significantly greater than the 6 AM bin. The 2020 C2S composite shows a definite morning peak in σ_{PV}, with an afternoon to evening minimum. Figure 4.4 also suggests a possible peak in σ_{PV}

in the midnight bin, but the peak cannot be said to be significant.

Hypothesized Greater Time-bin	Hypothesized Lesser Time-bin	Welch's t-test p-value returned
[9 PM – 3 AM) *(12 AM)*	[3 AM – 9 AM) *(6 AM)*	.278
[9 PM – 3 AM) *(12 AM)*	[9 AM – 3 PM) *(12 PM)*	.003 ***
[9 PM – 3 AM) *(12 AM)*	[3 PM – 9 PM) *(6 PM)*	.0007 ***

*** = significant on .01 alpha level

Table 4.3. Welch's one-sided t-test results for 2020 C2S.

It is important to note that each bin did not hold as many data points as one would hope when performing statistical tests. The midnight time-bin holds only 9 data points, whereas the 6 am, 12 PM, and 6 PM bins hold 10, 8, and 8 data points respectfully. Thus, these statistics cannot be said to be too conclusive. This led to the addition of more storms, and the creation of the 2020 – 2022 composite previously mentioned.

4.2.2.2. 2020 - 2022 Composite

The 2020 – 2022 composite increased the amount of data slightly, allowing for statistical statements to be a bit stronger. The midnight and 6 AM bins now hold 13 data points each, the 12 PM bin holds 12, and the 6 PM bin holds 14. Future work will be to add more data to each bin as the lab group expands the storm data sets. Slight changes are noticeable when comparing Fig. 4.5. to Fig. 4.4., where each of the violins plots look better filled-out. Both the medians and the means show a minimum in σ_{PV} found in the 12 PM bin (median = 8.0 PVU, mean = 8.4 PVU). Similar to the 2020 C2S composite, the midnight bin has the largest median (13.5 PVU) and mean (13.2 PVU). Overall, the distributions of data points in both the midnight and 6 AM bins are similar between the two composites. Statistical tests performed also show similar results to the tests performed on the 2020 C2S composite. An ANOVA test taken on the 2020 – 2022 C2S data also returned a significant p-value, suggesting that the means in at least two of the time

bins again differ significantly.

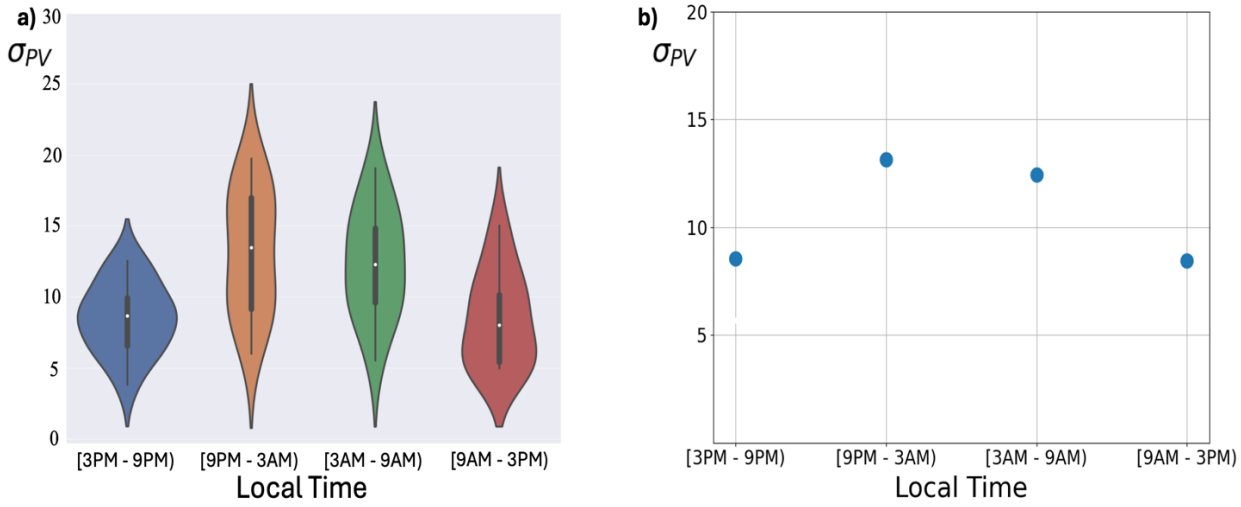

Figure 4.5. Violin Plot showing distribution of 2020 – 2022 C2S broken into four time bins. b) mean of σ_{PV} for each time bin.

Table 4.4 shows that when testing the midnight bin for the 2020 – 2022 C2S composite against the 12 PM and 6 PM bins, the mean of the midnight bin was significantly greater than that of the other two (p-values = 0.003 and 0.002, respectfully). However, the mean of the midnight bin again was not significantly greater than the mean of the 6 AM bin (p-value = 0.331) although it is slightly greater (13.2 PVU vs 12.5 PVU). Thus, similar statistical results were found when adding in the extra two years of data.

Hypothesized Greater Time-bin	Hypothesized Lesser Time-bin	Welch's t-test p-value returned
[9 PM – 3 AM) *(12 AM)*	[3 AM – 9 AM) *(6 AM)*	.331
[9 PM – 3 AM) *(12 AM)*	[9 AM – 3 PM) *(12 PM)*	.003 ***
[9 PM – 3 AM) *(12 AM)*	[3 PM – 9 PM) *(6 PM)*	.002 ***

*** = significant on .01 alpha level

Table 4.4. Welch's one-sided t-test results for the 2020 – 2022 C2S composite.

4.3. Annulus Method

Much of the previous research done on diurnal cycles has focused on radial propagation outward over the course of a day, stemming from work done by Dunion et al. (2014), which focuses on the cirrus canopy. Although it is hypothesized that σ_{PV} does not propagate outward in a similar fashion, due to PV dipoles being formed in the powerful updrafts of convection in tropical cyclones, it is important to show this.

To check for outward propagation, Welch's one-sided t-tests are again used to test statistical significance. Here it is expected that each ring would peak at separate times. Dunion et al.'s (2014) clock (see their Fig. 10) is used to pick which times each of the annuli would peak if σ_{PV} did propagate outwards like the cirrus canopy. Dunion et al. (2014) found a peak in IR cooling at a radius of 200 km right around sunrise (6 AM time-bin), and a peak at a radius of 300 km near noon (12 PM time-bin). They also found that there was not an evident cycle when looking at the innermost ring of 100 km (Dunion et al. 2014). In their paper, the authors also only looked at hurricanes that were category 2 or stronger, as they did not find a true cycle in weaker storms. So, this analysis will follow and only use the C2S composite when comparing.

4.3.1. Inner Ring

Unlike in Dunion et al.'s work with the cirrus canopy, Fig. 4.6 shows a discernable diurnal cycle for σ_{PV} in the inner ring (~ 100 km radii). The cycle of σ_{PV} for the inner ring seems to follow that of what was seen in the previous section when looking at σ_{PV} in both C2S composites, with a peak in σ_{PV} found around midnight. In both the 2020 C2S and 2020 – 2022 C2S composites, the mean of the midnight bin was significantly greater than both the 12 PM and 6 PM means, according to Table 4.5. In the 2020 – 2022 C2S composite, the mean of the

midnight bin was also significantly greater than that of the 6 AM bin, unlike what was found when looking at the whole storm domain.

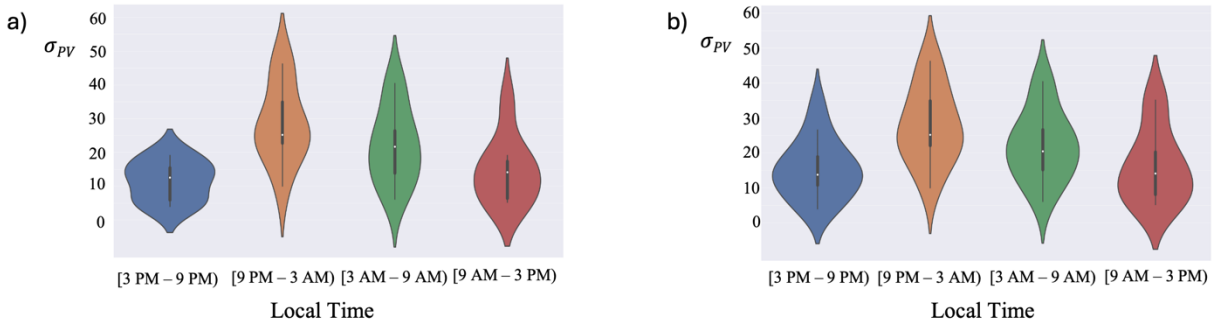

Figure 4.6. Violin plots for a) 2020 C2S inner ring, and b) 2020 – 2022 C2S inner ring.

Hypothesized Greater Time-bin	Hypothesized Lesser Time-bin	2020 p-value	2020-2022 p-value
[9 PM – 3 AM) *(12 AM)*	[3 AM – 9 AM) *(6 AM)*	.114	.089 *
[9 PM – 3 AM) *(12 AM)*	[9 AM – 3 PM) *(12 PM)*	.008 ***	.006 ***
[9 PM – 3 AM) *(12 AM)*	[3 PM – 9 PM) *(6 PM)*	.001 ***	.001 ***

* = significant on .10 alpha level
** = significant on .05 alpha level
*** = significant on .01 alpha level

Table 4.5. C2S inner ring significance testing.

4.3.2. Middle Ring

If σ_{PV} were to propagate outwards similar to the cirrus canopy in Dunion et al. (2014), σ_{PV} in the middle ring (~ 200 km) would peak in the 6 AM bin. Thus, when running statistical tests, the 6 AM mean was hypothesized to be greater than the means in the other three bins.

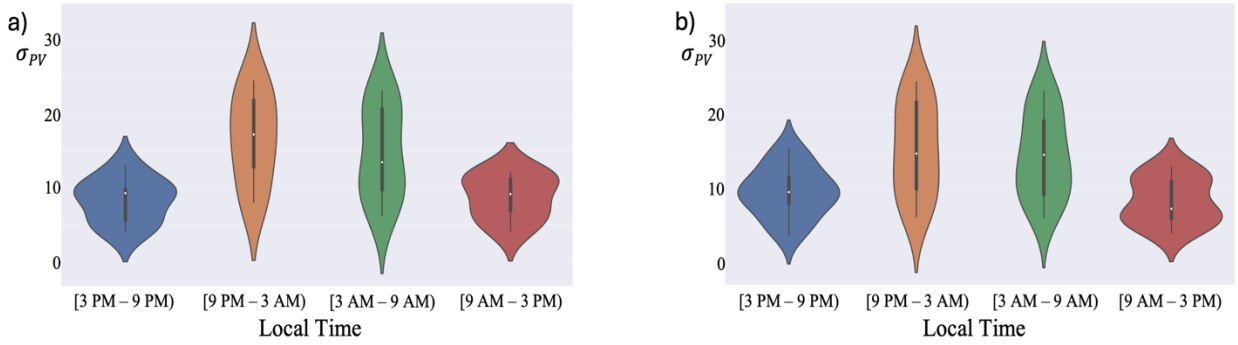

Figure 4.7. Violin plots for a) 2020 C2S middle ring and b) 2020 – 2022 C2S middle ring.

Compared to the inner ring, the diurnal cycle of the middle ring is much less recognizable (Fig. 4.7). Overall, the distribution of the 6 AM bin (hypothesized to be greater if the pattern of σ_{PV} were to propagate outward) does not look to be greater than that of the midnight bin. Significance testing shows that the mean of the 6 AM bin is greater than the means of the 12 PM and 6 PM bins. However, the p-values when comparing it to the midnight bin are very far from significant, and even suggest that the mean of the midnight bin is higher than the 6 AM bin for the middle ring. Thus, σ_{PV} in the middle ring does not peak with the cirrus canopy cycle found in Dunion et al. (2014). So far, both the inner and middle rings show similar diurnal cycles to the whole domain studied earlier. The inner ring has a bit more pronounced of a cycle than the whole domain, and the middle ring has a bit less recognizable diurnal cycle. Even with the lesser diurnal cycle, it is still clear that there is a strong peak in σ_{PV} early in the morning (midnight – 6 AM), which is significantly greater than the means in the afternoon/evening.

Hypothesized Greater Time-bin	Hypothesized Lesser Time-bin	2020 p-value	2020-2022 p-value
[3 AM – 9 AM) *(6 AM)*	[9 PM – 3 AM) *(12 AM)*	.729	.657
[3 AM – 9 AM) *(6 AM)*	[9 AM – 3 PM) *(12 PM)*	.009 ***	.002 ***
[3 AM – 9 AM) *(6 AM)*	[3 PM – 9 PM) *(6 PM)*	.006 ***	.007 ***

*** = significant on .01 alpha level

Table 4.6. C2S middle ring significance testing.

4.3.3 Outer Ring

If the diurnal cycle of σ_{PV} in the outer ring (~ 300 km) were to be the same as the diurnal cycle found in the cirrus canopy, it is hypothesized that the peak would be found in the 12 PM bin. Figure 4.8 shows a different story. The 6 AM time bin shows a clear peak in σ_{PV}. Statistics tell a similar story, with the p-value, when testing if the 12 PM bin has a greater mean than the 6 AM bin, was ≥ 0.950 (Table 4.7), suggesting that the 6 AM mean is significantly greater than the 12 PM mean. The 12 PM mean was also not greater than either the 6 AM or 6 PM means, thus σ_{PV}'s diurnal cycle in the outer ring is not the same as what is found in Dunion et al. (2014). Neither the diurnal cycle of σ_{PV} in the middle ring, or in the outer ring match that found with the cirrus canopy at similar radii around the center of a tropical cyclone. Thus, it is concluded that σ_{PV} does not propagate outwards similar to the cirrus canopy described in Dunion et al. (2014). This result aligns with our original hypothesis that a peak in σ_{PV} would not propagate outwards since PV dipoles in the UTLS are formed within convective updrafts (Hitchman and Rowe 2019, Jascourt 1997). This also aligns with why a strong diurnal cycle can be seen within the inner ring which aligns with the diurnal cycle of the whole domain in mature hurricanes. This does not set out to disprove Dunion et al.'s (2014) work with the cirrus canopy, as solar radiation differences throughout the day explains why the canopy propagates outwards after sunrise.

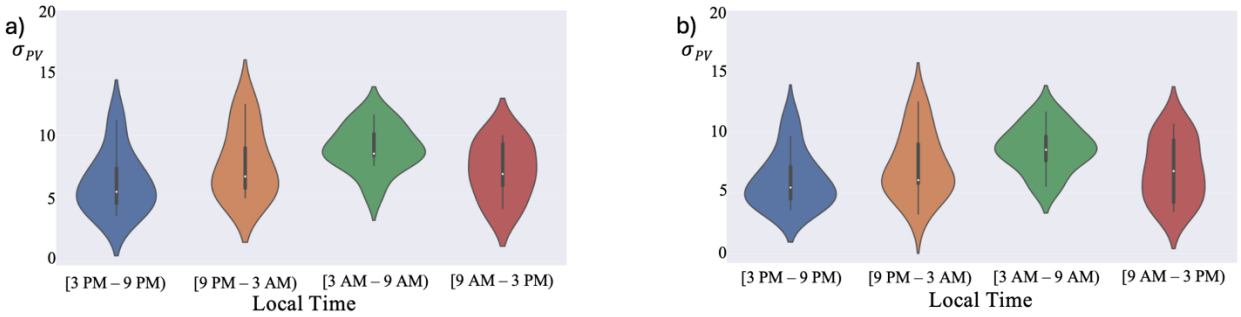

Figure 4.8. Violin plots for a) 2020 C2S outer ring and b) 2020 – 2022 C2S outer ring

Hypothesized Greater Time-bin	Hypothesized Lesser Time-bin	2020 p-value	2020-2022 p-value
[9 AM – 3 PM) *(12 PM)*	[9 PM – 3 AM) *(12 AM)*	.682	.660
[9 AM – 3 PM) *(12 PM)*	[3 AM – 9 AM) *(6 AM)*	.954	.972
[9 AM – 3 PM) *(12 PM)*	[3 PM – 9 PM) *(6 PM)*	.219	.203

Table 4.7. C2S outer ring significance testing.

4.4. Does Land Affect the Diurnal Cycle?

The last question to answer was one which I was intrigued about while reading Gray and Jacobson (1977) and Jiang et al. (2011). In both papers, a second peak in rainfall and convection was seen in the afternoon when the storms they studied were more over land. This led me to wonder, does landfall change the diurnal cycle of a hurricane? If so, is this change seen in σ_{PV}? To answer this question, new bins were made for both the 2020 – 2022 C1W and 2020 – 2022 C2S composites. Each bin created represented a different percentage that the storm was over land, using the ECMWF land mask variable. The first bin has times when each storm was almost entirely over ocean (0-10% over land). Then each bin following has times from each storm where they were progressively more over land. The second bin held data points where the storms were still mainly over the ocean (10-25% over land). The third and fourth were where the

storm was near 50% over land (25-50% over land, and 50-70% over land). The fifth and final bin was when the storm was mainly over land (75-100% over land). If the diurnal cycle of σ_{PV} were to change as a storm transitioned from over land to over ocean, then it would be expected that a peak later in the day would become more prominent in each of the C1W and C2S datasets.

4.4.1. C1W

When looking at non-mature hurricanes, it was found earlier that there was a slight peak seen in σ_{PV} near sunrise (6 am) that was not statistically significant, but is recognizable in Figs. 4.2. and 4.3. When dividing the 2020 – 2022 C1W time bins into the additional land mask bins, this peak is still evident (Fig. 4.9) in the mean of both land mask bins where the storms were mainly over water (0-10% and 10-25% over land). This peak then vanished when storms were partially over land. The mean of the 25 – 50% over land bin showed a clear peak that occurred in the 6 PM time bin, and the 50 – 75% over land bin showed a peak that occurred around midnight. In the 50 – 75% bin, σ_{PV} decreased over the course of the day, until around sunset, whereas in the 25 – 50% bin, the σ_{PV} increased throughout the whole day. Lastly, when storms were mainly over land (75 – 100% over land), the 6 AM peak was well-pronounced. This change in pattern could be due to the fact that the number of data points held in the 75 – 100% over land bin was just 24. When dividing that by the four time bins, this led to an average of six data points in each bin (max = 7, min = 4). Each of the other land mask bins held at least 42 data points.

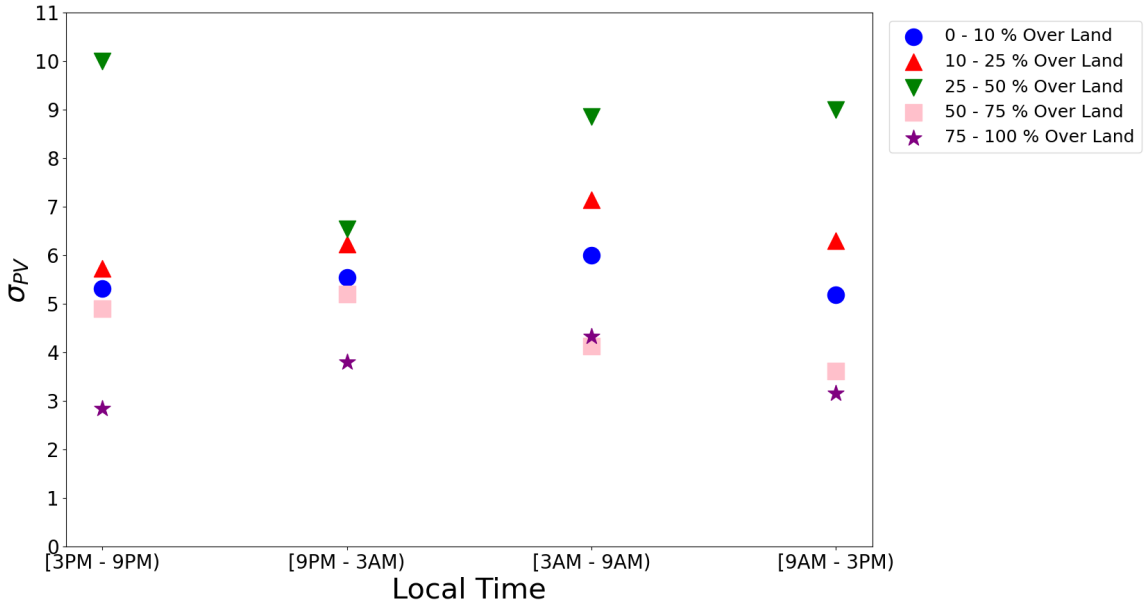

Figure 4.9. C1W diurnal cycle changes as percentage of storm shifts over land.

When looking at all the land mask bins except for the 75–100% over land bin. An afternoon to evening peak in σ_{PV} as a storm moves over land, similar to what was hypothesized. The 75 – 100 % over land bin clouds this result a bit, but also did not hold a significant amount of data. Another interesting takeaway is that σ_{PV} in all time bins are smaller when storms are greater than or equal to 50% over land.

4.4.2. C2S

Similar to the low data in the 75 – 100% over land bin when looking at the C1W composite, each of the land mask bins for C2S do not hold many data points. Due to this, the 50 – 75 % over land and 75 – 100 % over land bins are not used when looking at C2S. Even though there is the restraint of lower amounts of data, Fig 4.10 does show a later peak in σ_{PV} when these mature hurricanes are more over land. As was seen in the previous section, these mature hurricanes had a slight peak around midnight in σ_{PV}, although not statistically significant. When

storms were mainly over ocean, the peak in σ_{PV} occurred at midnight (Fig. 4.10), similarly to when looking at all storm times previously. However, when storms were more over land (25 – 50 % over land), this peak in σ_{PV} shifted to 6 AM.

Although there is a shift in where σ_{PV} peaks, this result for mature hurricanes does not seem to follow previous results on rainfall and convection found by Gray and Jacobson (1977) and Jiang et al. (2011). Two factors could be the reason for this discrepancy. The first is that there is not enough data for times when these storms in the Gulf of Mexico were classified as category 2 or stronger. Further expanding our data set to include more years of data hopefully would help this, but possibly not much. The second factor is that these mature hurricanes rarely make it this close to land. SSTs in the Gulf of Mexico drop off quite a bit prior to the shore, and these colder waters are not conducive for the storms to hold intensity.

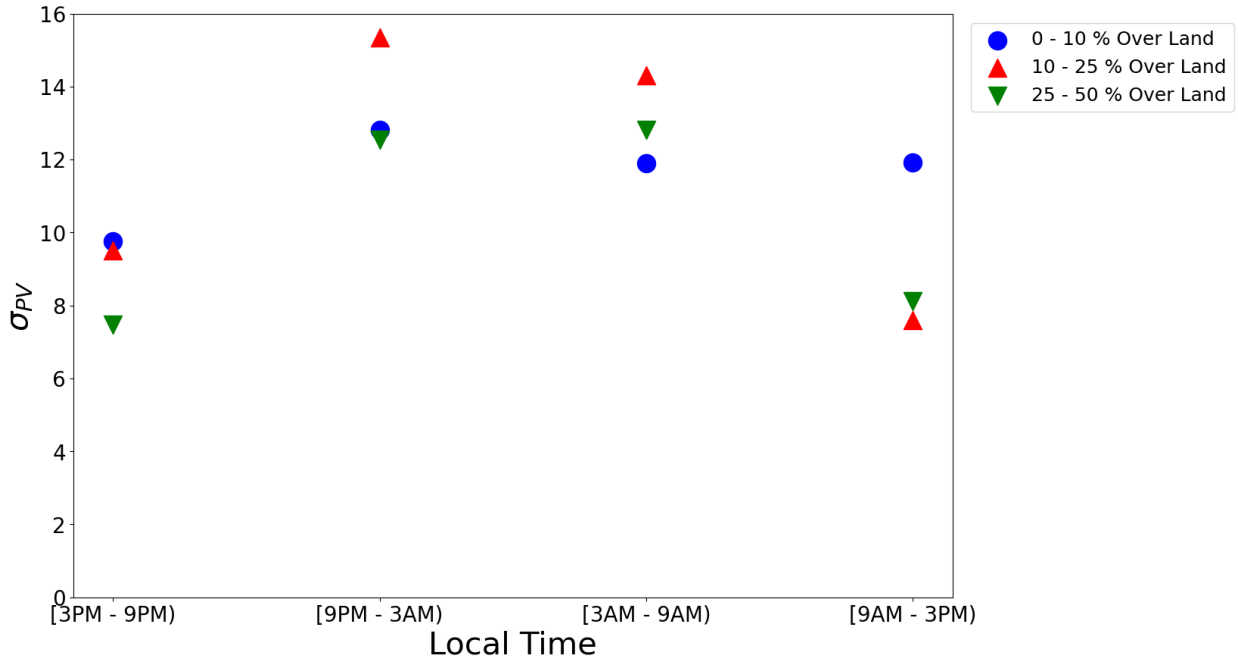

Figure 4.10. C2S diurnal cycle changes as percentage of storm shifts over land.

Chapter 5. Conclusions and Future Work

This study analyzed the diurnal cycle of potential vorticity variability (σ_{PV}) in the UTLS found in the ECMWF IFS High Resolution Operational Forecasts (ECMWF 2016). Three main hypotheses were tested.

1. The diurnal cycle of σ_{PV} in a mature hurricane (C2S) is different than that in a weaker hurricane (C1W), with the peak in σ_{PV} shifting closer to midnight, similar to work done by Ruppert and Hohenegger (2018).
2. σ_{PV} does not propagate radially outward over the course of a day, similar to the cirrus canopy cycle found in Dunion et al. (2014).
3. The diurnal cycle of σ_{PV} changes when a storm nears landfall, similar to results found in Gray and Jacobson (1977) and Jiang et al. (2011).

This study originally focused on just the 2020 Gulf of Mexico storms that reached an intensity of C1 at some point in their lifespan. However, the inclusion of 2021 and 2022 Gulf of Mexico storms allow for stronger statistical statements to be made.

It is concluded that a slight shift in the peak of σ_{PV} is found between weaker and more mature tropical cyclones. Figures show that there is a slight peak in σ_{PV} found closer to midnight in mature hurricanes, and one closer to sunrise in weaker hurricanes. However, statistical tests found that these peaks were not statistically significant (p-value > 0.10). Even though these tests did not prove a significant difference, the distributions in Figures 4.2 – 4.5 do show a slight shift in the cycle. A statistically significant peak in σ_{PV} at midnight is found when solely looking at the inner annulus in mature TCs. This peak can be attributed to stronger convection near the center of a storm. Also, in both C1W and C2S storms, the overnight and early morning values in σ_{PV} ([9 PM – 9AM)) are significantly greater than those found in the

late morning through evening times (p-value = 0.096 when analyzing if mean of C1W and C2S overnight and morning is greater than the mean C1W and C2S afternoon and evening data).

It is also concluded that σ_{PV} does not propagate outward similar to the cirrus canopy cycle in Dunion et al. (2014). The timing of the peak of σ_{PV} does not align with the timing of Dunion et al's. (2014) peak in IR brightness temperature. This result makes physical sense, as the cirrus canopy's outward propagation relies on solar radiation differences throughout the day, whereas potential vorticity anomalies must align within the convective updrafts, which remain more central. This also explains the statistically significant diurnal cycle found when looking at the inner ring of mature hurricanes. Strong updrafts and convection near the center of a hurricane creates stronger PV dipoles in the UTLS, leading to higher variability. The timing of this diurnal cycle also relates to Ruppert and Hohenegger's previous work using idealized models for convection (2018).

Lastly, it is also concluded from the C1W composite that the diurnal cycle of hurricanes does change as a storm is nearing landfall. This change in cycle was seen when an afternoon/evening peak in σ_{PV} became apparent in bins of data where storms were 25 – 75% over land. The same conclusions cannot be made currently when looking at the C2S composite due to lack of data.

This leads to future work. In the future, it would be beneficial to increase the composites with more data. The ECMWF data set used dates back to 2016, so the first step would be adding storms that went through the Gulf of Mexico during 2016 – 2019. Also, as the National Hurricane Center publishes new HURDAT data for 2023 and 2024 storms, these storms should also be included in the composites. Adding these additional years will start to help the problem of relatively small sample sizes.

Also, storms should be added from different basins in the future. Currently, there is a very narrow focus on the Gulf of Mexico, but the diurnal cycle found in these storms may not tell the full story of those found in other basins. Hitchman and Rowe (2024) shows similar results when looking at tropical cyclone Yasa in the South Pacific. It would be beneficial to combine results from all different ocean basins to narrate a more complete story of the tropical cyclone diurnal cycle.

Another interesting idea that could be studied in future projects is the effect of wind shear on azimuthal asymmetries over the open Atlantic Ocean, far from land. In tropical cyclone research, wind shear is a very widely discussed variable when looking at their life cycles. As far as I know, there are no papers that have tied wind shear to an effect on the diurnal cycle. Dunion et al (2014) used storms with low wind shear in their analysis. However, Leppert and Cecil (2016) found no significant difference in the diurnal cycle when comparing between low-shear storms versus storms with varying shear. It is expected that different levels of shear should not affect the diurnal cycle of σ_{PV}.

Although a pulsation outwards of σ_{PV} was not found in this work, it might be interesting to use annuli to analyze other segments of storms, including spiral rain bands, or normalizing annuli radii by storm size.

Bibliography

2020 Annual Report (2021). rep. London: AON. https://www.aon.com/getmedia/53674ecf-5d58-46d4-9e0c-5aa8e0d6f9cf/20210125-if-annual-cat-report.pdf

ABI Band 13 (10.3 μm) Quick Guide (no date) *CIMMS*. Available at: https://cimss.ssec.wisc.edu/goes/OCLOFactSheetPDFs/ABIQuickGuide_Band13.pdf.

Andrews, D. G., Holton, J. R., & Leovy, C. B. (1987), *Middle Atmosphere Dynamics*, Academic Press, 489 pp. https://doi.org/10.1002/qj.49711548612

Berg, R., and Reinhart, B. J., 2021: National Hurricane Center Tropical Cyclone Report: Hurricane Sally (11 September – 17 September 2020). Rep. AL192020, National Hurricane Center, 69 pp., https://www.nhc.noaa.gov/data/tcr/AL192020_Sally.pdf

Beven II, J. L., and Berg, R., 2021: National Hurricane Center Tropical Cyclone Report: Hurricane Marco (21 August – 25 August 2020). Rep. AL142020, National Hurricane Center, 31 pp., https://www.nhc.noaa.gov/data/tcr/AL142020_Marco.pdf.

Beven II, J. L., Hagen, A., and Berg, R., 2022: National Hurricane Center Tropical Cyclone Report: Hurricane Ida (26 August – 1 September 2021). Rep. AL092021, National Hurricane Center, 163 pp., https://www.nhc.noaa.gov/data/tcr/AL092021_Ida.pdf

Blackwell, J. (2020) *Record-breaking Atlantic hurricane season draws to an end*, *National Oceanic and Atmospheric Administration*. Available at: https://www.noaa.gov/media-release/record-breaking-atlantic-hurricane-season-draws-to-end#:~:text=In%20total%2C%20the%202020%20season,of%20111%20mph%20or%20greater).

Blake, E., 2023: National Hurricane Center Tropical Cyclone Report: Hurricane Lisa (31 October – 5 November 2022). Rep. AL152022, National Hurricane Center, 21 pp., https://www.nhc.noaa.gov/data/tcr/AL152022_Lisa.pdf

Blake, E., Berg, R., and Hagen, A., 2021: National Hurricane Center Tropical Cyclone Report: Hurricane Zeta (24 October – 29 October 2020). Rep. AL282020, National Hurricane Center, 56 pp., https://www.nhc.noaa.gov/data/tcr/AL282020_Zeta.pdf

Bowman, K. P., & Fowler, M. D. (2015), The diurnal cycle of precipitation in tropical cyclones. *J. Clim*., *28*, 5325–5334. https://doi.org/10.1175/JCLI-D-14-00804.1

Brown, D. P., Berg, R., and Reinhart, B. J., 2021: National Hurricane Center Tropical Cyclone Report: Hurricane Hanna (23 July – 26 July 2020). Rep. AL082020, National Hurricane Center, 49 pp., https://www.nhc.noaa.gov/data/tcr/AL082020_Hanna.pdf.

Bucci, L., Alaka, L., Hagen, A., Delgado, S., and Beven, J., 2023: National Hurricane Center Tropical Cyclone Report: Hurricane Ian (23 September – 30 September 2022). Rep. AL092022, National Hurricane Center, 70 pp., https://www.nhc.noaa.gov/data/tcr/AL092022_Ian.pdf

Cangialosi, J. P., and Berg, R., 2021: National Hurricane Center Tropical Cyclone Report: Hurricane Delta (4 October – 10 October 2020). Rep. AL262020, National Hurricane Center, 46 pp., https://www.nhc.noaa.gov/data/tcr/AL262020_Delta.pdf

Cangialosi, J.P., Delgado, S., and Berg, R., 2022: National Hurricane Center Tropical Cyclone Report: Hurricane Elsa (30 June – 9 July 2021). Rep. AL052021, National Hurricane Center, 70 pp., https://www.nhc.noaa.gov/data/tcr/AL052021_Elsa.pdf

Chagnon, J. M., & Gray, S. L. (2009), Horizontal potential vorticity dipoles on the convective storm scale. *Quart. J. Roy. Meteorol. Soc*., *135*, 1392–1408. https://doi.org/10.1002/qj.468

Dunion, J. P., Thorncroft, C. D., & Velden, C. S. (2014), The tropical cyclone diurnal cycle of mature hurricanes. *Mon. Wea. Rev.*, *142*, 3900-3919. doi:10.1175/MWR-D-13-00191.1

Duran, E. L., Berndt, E. B., & Duran, P. (2021), Observation of the tropical cyclone diurnal cycle using Hyperspectral Infrared Satellite Sounding Retrievals. *Mon. Wea. Rev*., *149(11),* 3671-3690. https://doi.org/10.1175/MWR-D-20-0415.1

European Centre for Medium-Range Weather Forecasts (2023), Integrated Forecast System Documentation – Cy48r1 Operational implementation 27 June 2023 PART III: Dynamics and numerical procedures, 40 pp. https://www.google.com/url?sa=t&rct=j&q=&esrc=s&source=web&cd=&ved=2ahUKEwj6sLKM-r-DAxUgmIkEHWxrDGEQFnoECBgQAQ&url=https%3A%2F%2Fwww.ecmwf.int%2Fsites%2Fdefault%2Ffiles%2Felibrary%2F2023%2F81369-ifs-documentation-cy48r1-part-iii-dynamics-and-numerical-pro

Evans, R. C., & Nolan, D. S. (2022), The spatiotemporal evolution of the diurnal cycle in two WRF simulations of tropical cyclones. *J. Atmos. Sci.*, *79*, 1021-1043. https://doi.org/10.1175/JAS-D-21-0100.1

Gray, W. M., & Jacobson Jr, R. W. (1977). Diurnal variation of deep cumulus convection. *Monthly Weather Review*, *105*, (9), 1171 – 1188.

Hitchman, M. H. and S. M. Rowe, Diagnosing the evolution and diurnal cycle of tropical cyclone Yasa using potential vorticity from ECMWF High-Resolution Operational Forecasts. *J. Atmos. Sci*. (2024), submitted.

Hitchman, M. H., & Rowe, S. M. (2019), On the structure and formation of UTLS PV dipole/jetlets in tropical cyclones by convective momentum surges. *Mon. Wea. Rev., 147*, 4107-4125. https://doi.org/10.1175/MWR-D-18-0232.1

Holland, G. J., and R. T. Merrill, 1984: On the dynamics of tropical cyclone structural changes. *Quart. J. Roy. Meteor. Soc.*, **110**, 723–745, https://doi-org.ezproxy.library.wisc.edu/10.1002/qj.49711046510.

Hunter, J.D., (2007). Matplotlib: A 2D Graphics Environment, *Computing in Science & Engineering*, *vol. 9*, no. 3, pp. 90-95.

Jarvinen, B. R., C. J. Neumann, and M. A. S. Davis, 1984: A tropical cyclone data tape for the North Atlantic Basin, 1886-1983: Contents, limitations, and uses. NOAA Technical Memorandum NWS NHC 22, Coral Gables, Florida, 21 pp. http://www.nhc.noaa.gov/pdf/NWS-NHC-1988-22.pdf

Jascourt, S. D. (1997), *Convective organizing and upscale development processes explored through idealized numerical experiments.* Ph.D. dissertation, University of Wisconsin-Madison, 267 pp. https://www.proquest.com/pqdtlocal1006298/results/CD0E6E5D92794CEBPQ/1?accountid=465

Jiang, H., C. Liu, and E. J. Zipser, 2011: A TRMM-Based Tropical Cyclone Cloud and Precipitation Feature Database. *J. Appl. Meteor. Climatol.*, *50*, 1255–1274, https://doi-org.ezproxy.library.wisc.edu/10.1175/2011JAMC2662.1.

Latto, A. S., 2021: National Hurricane Center Tropical Cyclone Report: Hurricane Gamma (2 October – 6 October 2020). Rep. AL252020, National Hurricane Center, 20 pp., https://www.nhc.noaa.gov/data/tcr/AL252020_Gamma.pdf

Latto, A. S., and Berg, R., 2022: National Hurricane Center Tropical Cyclone Report: Hurricane Nicholas (12 September – 15 September 2021). Rep. AL142021, National Hurricane Center, 50 pp., https://www.nhc.noaa.gov/data/tcr/AL142021_Nicholas.pdf

Leppert, K.D. & Cecil, D.J. (2016) Tropical cyclone diurnal cycle as observed by TRMM. *Monthly Weather Review*, 144(8), 2793–2808. Available from: https://doi-org.ezproxy.library.wisc.edu/10.1175/mwr-d-15-0358.1

Melhauser, C., & Zhang, F. (2014), Diurnal radiation cycle impact on the pregenesis environment of Hurricane Karl (2010). *J. Atmos. Sci.*, *71*, 1241–1259. https://doi.org/10.1175/JAS-D-13-0116.1

Mishra, P., Singh, U., Pandey, C. M., Mishra, P., and Pandey, G. (2019). Application of student's t-test, analysis of variance, and covariance. Annals of Cardiac Anaesthesia. 22. 407. 10.4103/aca.ACA_94_19.

Navarro, E. L., and Hakim, G. J. (2016), Idealized numerical modeling of the diurnal cycle of tropical cyclones. *J. Atmos. Sci*., *73*, 4189–4201. https://doi.org/10.1175/JAS-D-15-0349.1

Pasch, R. J., Berg, R., Roberts, D. P., and Papin, P. P., 2021: National Hurricane Center Tropical Cyclone Report: Hurricane Laura (20 August – 29 August 2020). Rep AL132020, National Hurricane Center, 75 pp., https://www.nhc.noaa.gov/data/tcr/AL132020_Laura.pdf

Pasch, R. J., Reinhart, B. J., Berg, R., and Roberts, D. P., 2021: National Hurricane Center Tropical Cyclone Report: Hurricane Eta (31 October – 13 November 2020). Rep. AL292020, National Hurricane Center, 70 pp., https://www.nhc.noaa.gov/data/tcr/AL292020_Eta.pdf

Probst, P., Annunziato, A., Proietti, C., Paris, S., Atlantic Hurricane Season: A record-breaking season, EUR30635 EN, Publications Office of the European Union, Luxembourg, (2021). ISBN 978-92-76-32177-4, doi:10.2760/00114, JRC123932.

Reed, K.A., Wehner, M.F. & Zarzycki, C.M., Attribution of 2020 hurricane season extreme rainfall to human-induced climate change. Nat Commun 13, 1905 (2022). https://doi-org.ezproxy.library.wisc.edu/10.1038/s41467-022-29379-1

Reinhart, B. J., Reinhart A., and Berg, R., 2022: National Hurricane Center Tropical Cyclone Report: Hurricane Grace (13 August – 21 August 2021). Rep. AL072021, National Hurricane Center, 49 pp., https://www.nhc.noaa.gov/data/tcr/AL072021_Grace.pdf

Ruppert, J. H., & Hohenegger, C. (2018). Diurnal circulation adjustment and organized deep convection. Journal of Climate, 31 (12), 4899 – 4916. doi: 10.1175/JCLI-D-17-0693.1.

Ruppert, J. H., & O'Neill, M. E. (2019), Diurnal cloud and circulation changes in simulated tropical cyclones. *Geophys. Res. Lett.*, *46*, 502-511. 10.1029/2018GL081302

Stewart, S. R., 2021: National Hurricane Center Tropical Cyclone Report: Hurricane Iota (13 November – 18 November 2020). Rep. AL312020, National Hurricane Center, 48 pp., https://www.nhc.noaa.gov/data/tcr/AL312020_Iota.pdf

Student (1908) The Probable Error of a Mean. Biometrika, 6, 1-25. http://dx.doi.org/10.1093/biomet/6.1.1

Van Rossum, G., & Drake, F. L. (2009). *Python 3 Reference Manual*. Scotts Valley, CA: CreateSpace.

Virtanen, P., Gommers, R., Oliphant, T. E., Haberland, M., Reddy, T., Cournapeaue, D., Burovski, E., Peterson, P., Weckesser, W., Bright, J., van der Walt, S. J., Brett, M., Wilson, J., Millman, K. J., Mayorov, N., Nelson, A. R. J., Jones, E., Kern, R., Larson, Eric., Carey, C.J., Polat, I., Feng, Y., Moore, E.W., VanderPlas, J., Laxalde, D., Perktold, J., Cimrman, R., Henriksen, I., Quintero, E.A., Harris, C. R., Archibald, A. M., Ribeiro, A. H., Pedregosa, F., van Mulbregt, P., and SciPy 1.0 Contributors. (2020) SciPy 1.0: Fundamental Algorithms for Scientific Computing in Python. *Nature Methods*, *17*(3), 261 – 272.

Waskom, M. L., (2021). seaborn: statistical data visualization. *Journal of Open Source Software, 6*(60), 3021, https://doi.org/10.21105/joss.03021.

Welch, B. L. (1938). The Significance of the Difference Between Two Means when the Population Variances are Unequal. *Biometrika*, *29*(3/4), 350–362. https://doi.org/10.2307/2332010

West RM. Best practice in statistics: Use the Welch *t*-test when testing the difference between two groups. Ann Clin Biochem. 2021 Jul;58(4):267-269. doi: 10.1177/0004563221992088. Epub 2021 Feb 9. PMID: 33562996.

Wu, Q., and Ruan, Z. (2016). Diurnal variations of the areas and temperatures in tropical cyclone clouds. *Quarterly Journal of the Royal Meteorological Society*, **142**(700), 2788–2796. https://doi-org.ezproxy.library.wisc.edu/10.1002/qj.2868